AD_____

Award Number: W81XWH-F€ÈGÈ€Í I

TITLE: Ùc^{ ÁÕ^||ÁV@¦æ]^Á[¦ÁP^æ]ã*ÁV[¨}å^åÁÙ\ã}Áæ}åÁÙ[¬åVã•ˇ^•

PRINCIPAL INVESTIGATOR: Ö¦ÊÃ�sæ¡ÁÁ}ÍÃ^ˇ}*

CONTRACTING ORGANIZATION: V@¦Õ^}^çæ¦Ç[¨}åæ]}ÊÃÁÁ^¸[[åÊ¦Y Œ¦ÁÎ IJJ

REPORT DATE: R¨|˄Á€FG

TYPE OF REPORT: Annual

PREPARED FOR: U.S. Army Medical Research and Materiel Command
                        Fort Detrick, Maryland 21702-5012

DISTRIBUTION STATEMENT: Approved for public release; distribution unlimited

REPORT DOCUMENTATION PAGE

Public reporting burden for this collection of information is estimated to average 1 hour per response, including the time for reviewing instructions, searching existing data sources, gathering and maintaining the data needed, and completing and reviewing this collection of information. Send comments regarding this burden estimate or any other aspect of this collection of information, including suggestions for reducing this burden to Department of Defense, Washington Headquarters Services, Directorate for Information Operations and Reports (0704-0188), 1215 Jefferson Davis Highway, Suite 1204, Arlington, VA 22202-4302. Respondents should be aware that notwithstanding any other provision of law, no person shall be subject to any penalty for failing to comply with a collection of information if it does not display a currently valid OMB control number. **PLEASE DO NOT RETURN YOUR FORM TO THE ABOVE ADDRESS.**

1. REPORT DATE *(DD-MM-YYYY)* 01-07-2012	2. REPORT TYPE Annual	3. DATES COVERED *(From - To)* 15 JUN 2011 - 14 JUN 2012
4. TITLE AND SUBTITLE Stem Cell Therapy for Healing Wounded Skin and Soft Tissues		**5a. CONTRACT NUMBER**
		5b. GRANT NUMBER W81XWH-10-2-0054
		5c. PROGRAM ELEMENT NUMBER
6. AUTHOR(S) Dr. Kai P. Leung E-Mail: KAI.LEUNG@US.ARMY.MIL		**5d. PROJECT NUMBER**
		5e. TASK NUMBER
		5f. WORK UNIT NUMBER
7. PERFORMING ORGANIZATION NAME(S) AND ADDRESS(ES) The Geneva Foundation Lakewood, WA 96499		**8. PERFORMING ORGANIZATION REPORT NUMBER**
9. SPONSORING / MONITORING AGENCY NAME(S) AND ADDRESS(ES) U.S. Army Medical Research and Materiel Command Fort Detrick, Maryland 21702-5012		**10. SPONSOR/MONITOR'S ACRONYM(S)**
		11. SPONSOR/MONITOR'S REPORT NUMBER(S)

12. DISTRIBUTION / AVAILABILITY STATEMENT

Approved for Public Release; Distribution Unlimited

13. SUPPLEMENTARY NOTES

14. ABSTRACT

Profiling of Paracrine Factors Secreted by Leporine-deprived Mesenchymal Stem Cells

15. SUBJECT TERMS

Adipose-deprived mesenchymal stem cells; cytokines; paracine factors

16. SECURITY CLASSIFICATION OF:			17. LIMITATION OF ABSTRACT	18. NUMBER OF PAGES	19a. NAME OF RESPONSIBLE PERSON USAMRMC
a. REPORT U	**b. ABSTRACT** U	**c. THIS PAGE** U	UU	74	**19b. TELEPHONE NUMBER** *(include area code)*

Table of Contents

INTRODUCTION:

Exogenously applied stem cells can integrate into wounds, and if properly directed to regenerate tissue rather than to rapidly restore the barrier function, should be able to regenerate tissue for improved wound healing. We hypothesize that when applied topically to wounds, adult, adipose-derived mesenchymal stem cells that are directed toward tissue regeneration can reduce inflammation, increase angiogenesis, reduce scarring, and improve the restoration of skin functions. The goal of the proposed research is to define the function of stem cells alone or in matrix to promote healing by regeneration to improve wound repair outcomes.

BODY

I. Effect of rabbit MSCs on wound healing.

### 1. Determination of the optimal number of rabbit adipose-derived stem cells (ASCs) to promote wound healing

We treated wounds with different amounts of ASCs to determine the optimal quantity to promote wound healing. Saline was used as the vehicle to deliver ASCs. Previous work in the laboratories has shown that the use of fibrin sealant and hydrogels as vehicles do not have added any beneficial effects in promoting wound healing. An early passage (P3) ASCs was used in these experiments. This is to avoid changes of ASC surface markers due to repetitive *in vitro* sub-culturing. ASCs were harvested, washed in PBS to remove cell culture medium, and resuspended in PBS. Three different amounts of ASCs -3×10^5, 1×10^5, and 3×10^4 - in 7 µl of PBS- were delivered to each 7 mm wound of one of the ears. In the contralateral ear, 7 µl of PBS was delivered to each wound as a control. Wounds were harvested at Post-operative Day (POD) 7 and wound healing parameters such as epithelial and granulation tissue distances and areas were digitally quantified from histological sections of the control wounds and wounds that were treated with ASCs.

ASC treated wounds showed increased granulation tissue distance and granulation tissue area when compared to saline treated wounds (Figure 1B, C). Statistical significance of granulation tissue formation was found in wounds treated with the lowest number of ASCs (3×10^4 ASCs). A minor inhibition of keratinocyte migration was observed in wounds that were treated with larger quantities of ASCs (Figure 1A). However, this minor inhibition of keratinocytes migration was not statistically significant.

1
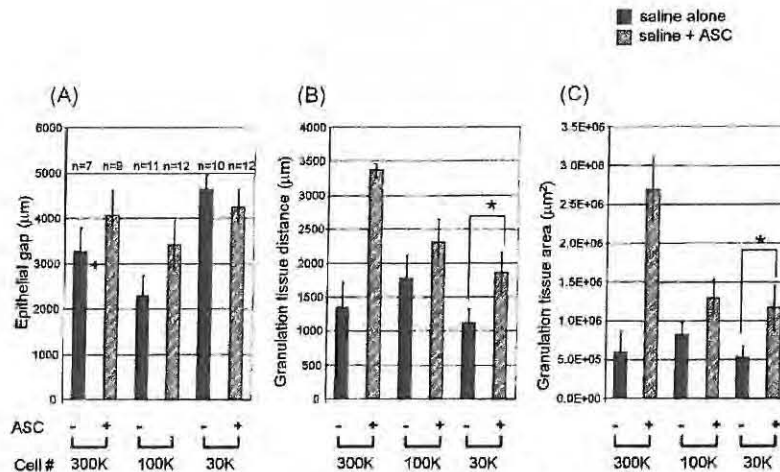
Figure 1. Histological quantification of ASCs treated wounds. Three different quantities of ASCs (3×10^5, 1×10^5, or 3×10^4) in PBS were delivered to each 7 mm wound of one ear in each test animal. In the contra lateral ear, PBS alone was delivered as a control. Wounds were harvested at POD 7 and epithelial gap (A), granulation tissue distance (B), and granulation tissue area (C) were measured. Data were shown as mean $\pm$ SEM. *p<0.05.

To determine the dose of ASCs which does not inhibit epithelialization yet able to increase granulation tissue formation, wounds on each one of the ear in the test animals were treated with either 1×10^5 ASCs or 3×10^4 ASCs. Wounds transplanted with 1×10^5 ASCs (n=11) had similar epithelial gaps (Figure 2A, $4,351 \pm 423$ μm) as compared to wounds with 3×10^4 ASCs (n=12, $4,085 \pm 322$ μm). However, wounds treated with 1×10^5 ASCs showed a greater granulation tissue distance (Figure 2B, $1,944 \pm 315$ vs. $1,454 \pm 221$ μm, p = 0.054) and the granulation tissue area (Figure 2C, $1,482,334 \pm 214,419$ vs. $950,926 \pm 128,948$ μm^2, p =0.09).
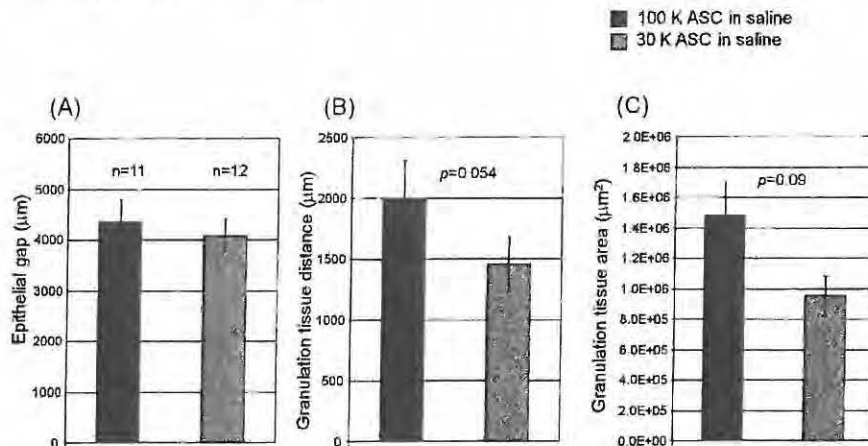
Figure 2. Histological quantification of ASC-treated wounds. 1×10^5 ASCs were delivered to 7 mm wounds on one of the ears and 3×10^4 ASCs were delivered to wounds on the contralateral ear of the test animals. Wounds were harvested at POD7 and epithelial gap (A), granulation tissue distance (B), and granulation tissue area (C) were measured. Data were shown as mean $\pm$ SEM.

2

It has been shown that ASCs secrete many cytokines and growth factors which are known to promote wound healing. We investigated whether ASCs can promote wound healing by the expression of these factors without proliferation or transdifferentiation to other cells. ASCs were treated with 10 µg/ml of Mitocmycin C (MitC) for 3 hours *in vitro* before harvest for application to wounds. Because MitC-treated ASCs are viable but unable to proliferate, higher concentration of ASCs was delivered to wounds to ensure an adequate secretion of growth factors. Histological analysis showed that wounds with MitC-treated ASCs had decreased granulation tissue distance (data not shown) and granulation tissue area (Figure 3B). Interestingly, increased epithelialization was found in wounds containing 1×10^5 MitC-treated ASCs versus wounds containing 1×10^5 of ASCs without MitC (Figure 3A; $4,258 \pm 335$ µm vs. $3,060 \pm 489$ µm, respectively; p =0.07).
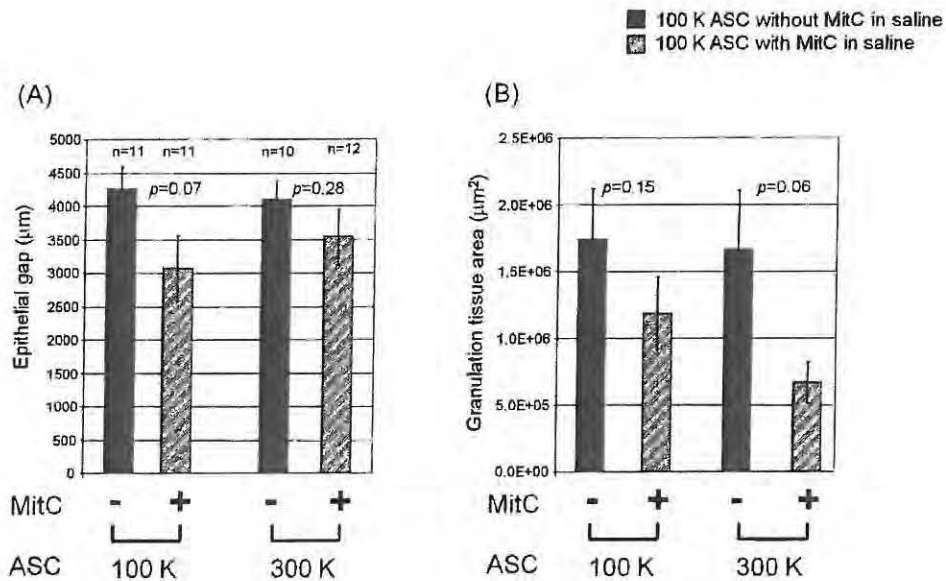
Figure 3. Histological quantification of wounds treated with growth-arrested ASCs. ASCs (1×10^5 or 3×10^5 per 7 mm wound) were treated with MitC (10 µg/ml) for 3 hours *in vitro* before delivery to wounds. ASCs without MitC treatment were delivered to wounds on the contralateral ear of each teat rabbit for comparison. Wounds were harvested at POD7 and epithelial gap (A) and granulation tissue area (B) were measured. Data were shown as mean $\pm$ SEM.

2. Effects of rabbit mesenchymal stem cells (MSCs) on wound healing

We determined that saline was the optimal MSC delivery vehicle and 1×10^5 ASCs was the optimum number of ASCs to promote wound healing. To increase the power of statistical analyses, we increased the number of animals (and wounds) and compared the treated versus control wounds on the same animal to minimize the effects of rabbit-to-rabbit variation in wound healing.

2.1. Effects of ASCs on wound healing

P3 ASCs were harvested, washed in PBS, and resuspended in PBS. 1×10^5 ASCs in 7 µl of PBS were delivered to each 7mm wound on one of the ears in rabbits. PBS (7

3

µl; contrl) was applied to wounds on the contralateral ear. Wounds were harvested at POD7. Treatment with ASCs (n=36) did not affect epithelialization when compared to saline treated wounds (n=35) (Figure 4A; 3,913 ± 259 µm vs. 4,026 ± 306 µm, respectively; p =0.8). However, granulation tissue distance (1,748 ± 165 µm vs. 1,170 ± 147 µm, respectively, p <0.01) and granulation tissue area (1,133,933 ± 135,864 µm² vs. 503,530 ± 71,984 µm²; p <0.001) were significantly increased by ASCs treatment (Figure 4B, C).
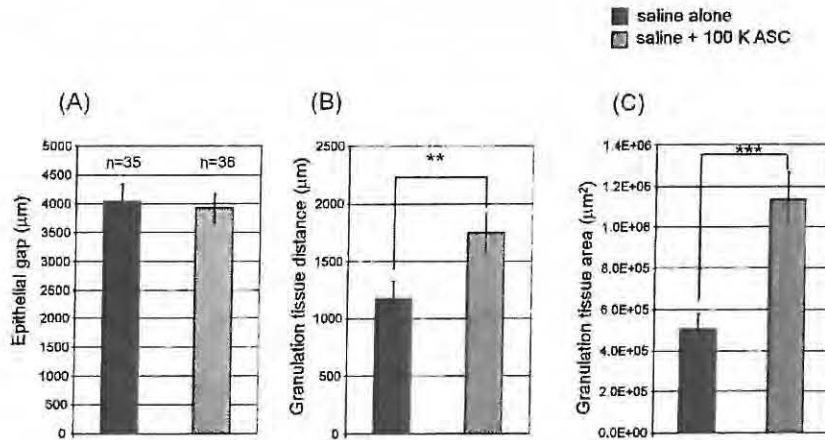
Figure 4. **Histological quantification of ASCs treated wounds.** 1 x 10⁵ ASCs in PBS was delivered to the 7 mm wounds. PBS alone was used as the vehicle control. Wounds were harvested at POD7 and epithelial gap (A), granulation tissue distance (B), and granulation tissue area (C) were measured. Data were shown as mean ± SEM. **p<0.01, ***p<0.001.

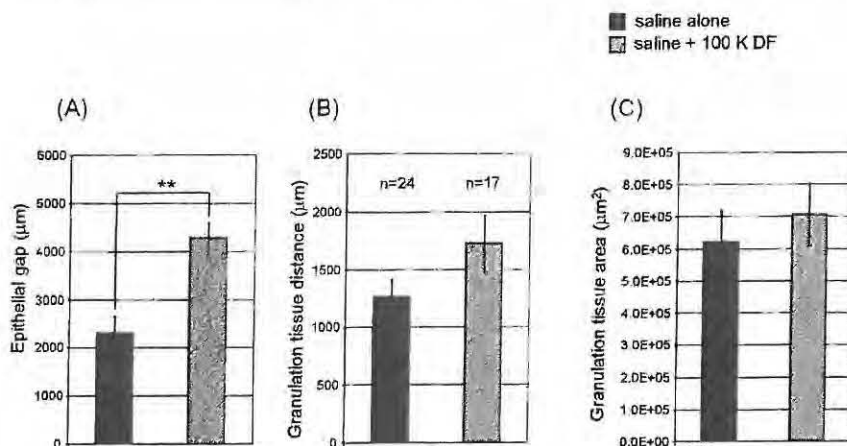## 2.2. Effects of bone marrow (BM) derived-MSCs on wound healing

P3 BM-MSCs were harvested, washed in PBS, and resuspended in PBS. Each 7 mm wound of one of the ears of animals was treated with 1 x 10⁵ BM-MSCs in 7 µl of PBS. In the contralateral ear, 7 µl of PBS was delivered to each wound as a control. Wounds were harvested at POD7. Treatment with BM-MSCs (n=20) inhibited epithelialization as compared to saline-treated wounds (n=17) (Figure 5A, 4,552 ± 243 µm vs. 2,765 ± 360 µm, respectively; p <0.01). Granulation tissue distance (2,283 ± 249 µm vs. 1,435 ± 212 µm, respectively; p <0.001) was increased in the treated wounds, although granulation tissue area (1,152,142 ± 133,463 µm² vs. 961,843 ± 322,652 µm² respectively; p = 0.72) was not significantly different from that of the control wounds (Figure 5B, C).
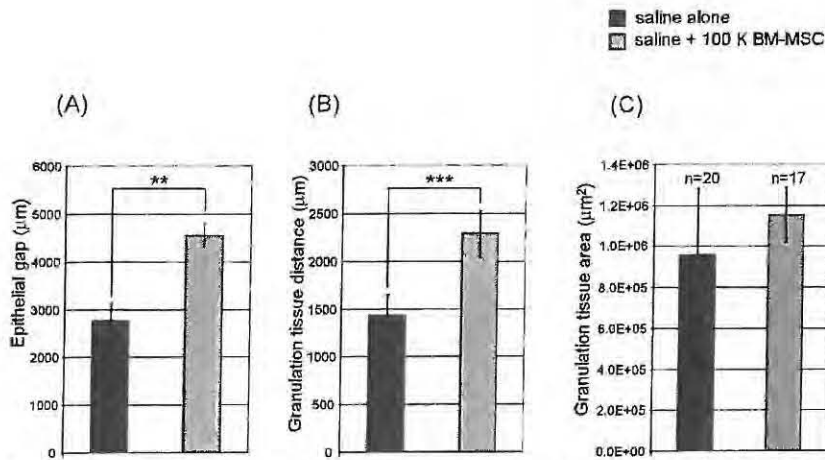
Figure 5. Histological quantification of BM-MSCs treated wounds. 1×10^5 BM-MSCs in PBS was delivered to each 7 mm wound. PBS was used as the treatment control. Wounds were harvested at POD7 and epithelial gap (A), granulation tissue distance (B), and granulation tissue area (C) were measured. Data were shown as mean $\pm$ SEM. **p<0.01, ***p<0.001.

2.3. Effect of dermal fibroblasts (DFs) on wound healing

P3 DFs were harvested, washed in PBS, and resuspended in PBS. Each 7 mm wound of one the ears was treated with 1×10^5 DFs in 7 μl of PBS. In the contralateral ear, 7 μl of PBS per wound were delivered as a control. Wounds were harvested at POD7. Treatment with DFs (n=24) inhibited epithelialization as compared to saline-treated wounds (n=17) (Figure 6A, $4,279 \pm 317$ μm vs $2,304 \pm 347$ μm, respectively; p <0.01). Neither granulation tissue distance ($1,719 \pm 244$ μm vs. $1,262 \pm 153$ μm; p = 0.13) nor granulation tissue area ($703,357 \pm 97,286$ vs. $623,852 \pm 96,976$ μm^2; p = 0.45) was significantly changed in treated versus control wounds (Figure 6B, C).

Figure 6. Histological quantification of DFs treated wounds. 1×10^5 DFs in PBS was delivered to 7 mm wounds on one ear. In the contralateral ear, PBS alone was delivered as a control. Wounds were harvested at POD7 and epithelial gap (A), granulation tissue distance (B), and granulation tissue area (C) were measured. Data were shown as mean $\pm$ SEM. **p<0.01.

2.4. Effect of growth-arrested rabbit ASCs (MitC-ASCs) on wound healing

P3 ASCs were treated with 10 µg/ml of MitC for 3 hours, harvested, washed in PBS, and resuspended in PBS. Each 7 mm wound of one ear was treated with 1 x 10^5 MitC-treated ASCs in 7 µl of PBS. In the contralateral ear, 7 µl of PBS were delivered to each wound as a control. Wounds were harvested at POD7. Treatment with MitC-treated ASC (n=23) did not affect epithelialization of epidermis when compared to saline treated wounds (n=24) (Figure 7A, 3,426 ± 240 µm vs. 2,873 ± 279 µm, respectively; p =0.17). Neither granulation tissue distance (1,346 ± 155 µm vs. 1,670 ± 194 µm, respectively; p = 0.17) nor granulation tissue area (983,928 ± 248,884 $µm^2$ vs. 990,601 ±171,666 $µm^2$, respectively; p = 0.93) was significantly changed (Figure 7, C).
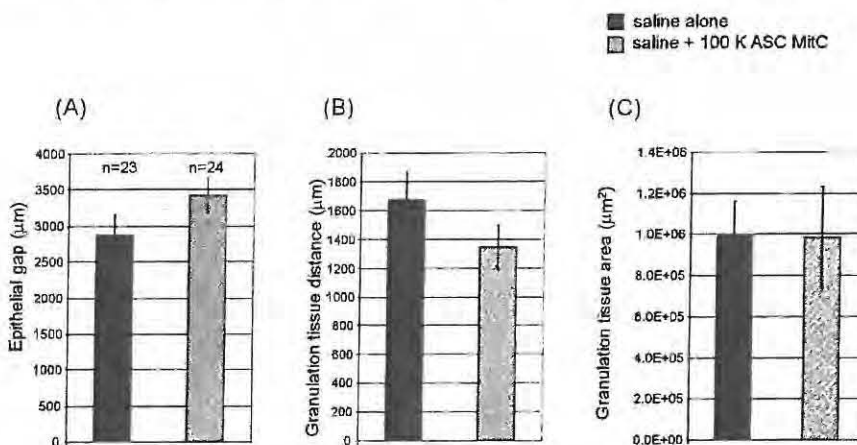

Figure 7. Histological quantification of wounds treated with growth arrested ASCs (MitC-ASCs). 1 x 10^5 MitC-ASCs in PBS was delivered to each of the 7 mm wounds on one ear. In the contralateral ear, PBS alone was delivered as the control. Wounds were harvested at POD7 and epithelial gap (A), granulation tissue distance (B), and granulation tissue area (C) were measured. Data were shown as mean ± SEM.

3. Analysis of transplanted rabbit ASCs

### 3.1. Transplanted ASCs exhibit activated fibroblast phenotype

ASCs can contribute to wound healing either by the expression and secretion of cytokines/growth factors or differentiation and repopulation of the wound bed. The fate (or characteristics) of transplanted ASCs was addressed using the green fluorescent protein (GFP)-expressing ASCs (GFP-ASC). A total of 1×10^5 GFP-ASCs in saline was delivered as described above. Wounds were harvested at POD 7 and histological analyses were performed. Immunofluorescence staining with chicken anti-GFP antibody showed that transplanted ASCs were evenly distributed in the wound bed and granulation area (Figure 8A & 9A). During the wound repair process, fibroblasts migrate to the wound site and build up granulation tissue by depositing collagen and other extracellular matrices. These activated myofibroblasts are α-SMA (smooth muscle actin) positive. Immunofluorescence staining with mouse anti-α-SMA antibody detected endogenously activated fibroblasts (Figure 8B, B'). Interestingly, the majority of transplanted ASCs showed α-SMA signals (Figure 8C, C', D, D'). We also observed ASCs which do not express α-SMA (arrowhead in Figure 8D').
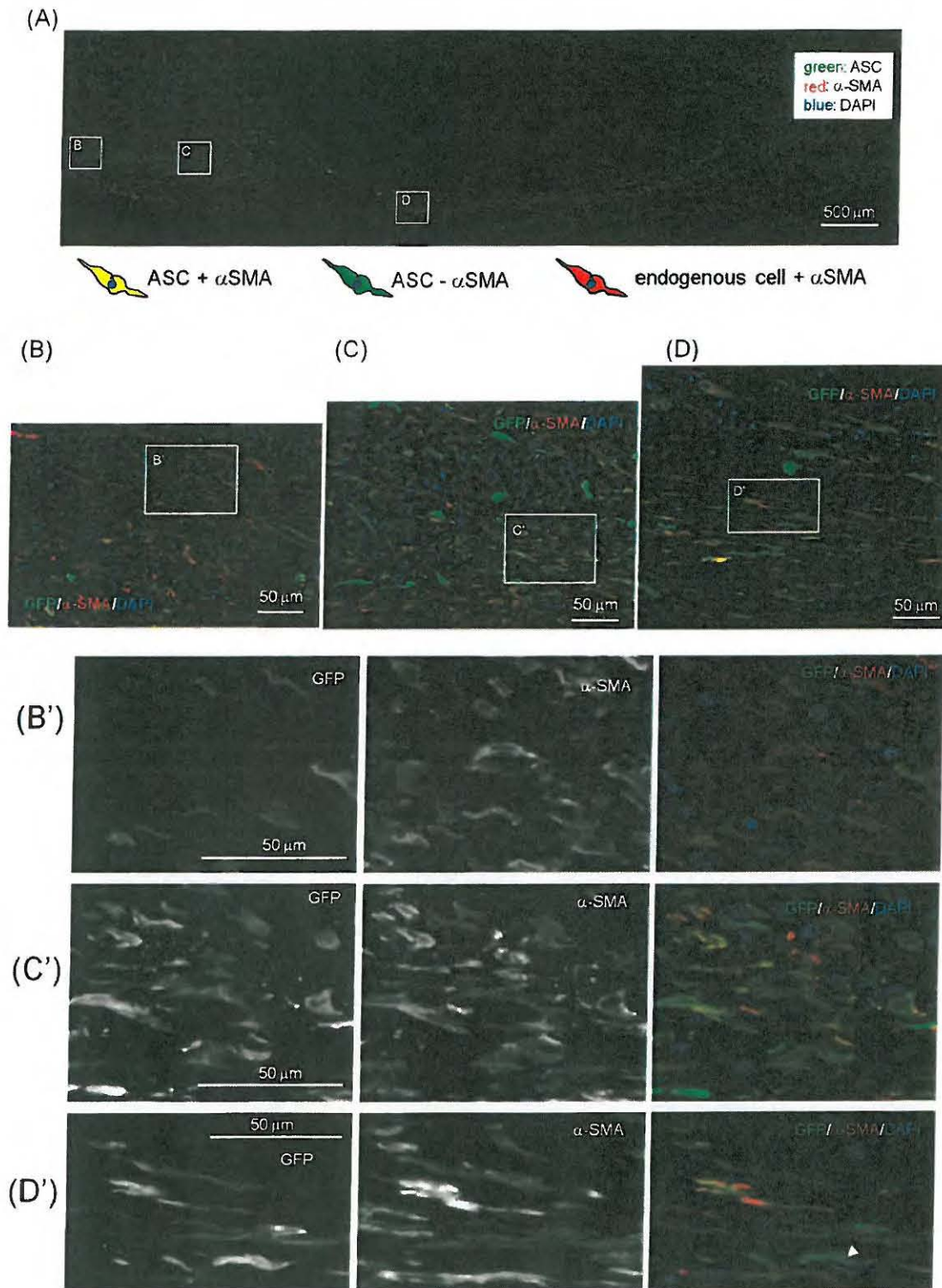
Figure 8. Transplanted GFP-ASCs express α-SMA in wounds. Rabbit ear wounds at POD7 were stained with chicken anti-GFP and mouse anti-α-SMA antibodies. Nuclei were stained with DAPI. Merged image of α-SMA (red) and GFP (green) indicates that α-SMA is expressed in ASCs. (A) A lower magnification of the wound. (B-D) Higher magnifications of the indicated regions (white squares) in A.

7

(B'-D') Higher magnifications of the indicated regions in B-D. Scale bars: 500 μm (A), 50 μm (B, C, D, B', C', D').

We next analyzed the expression of collagen III (Col III), which is produced by myofibroblasts prior to the synthesis of the mechanically stronger collagen I. It has been shown that fetal dermis, which forms less scar upon injury, has elevated level of Col III. Expression of Col III was detected outside of the wounding area (Figure 9B). Expression of Col III was also detected in the wound bed (Figure 9C, C') and granulation tissue (Figure 9D, D'), though the signal was weak.
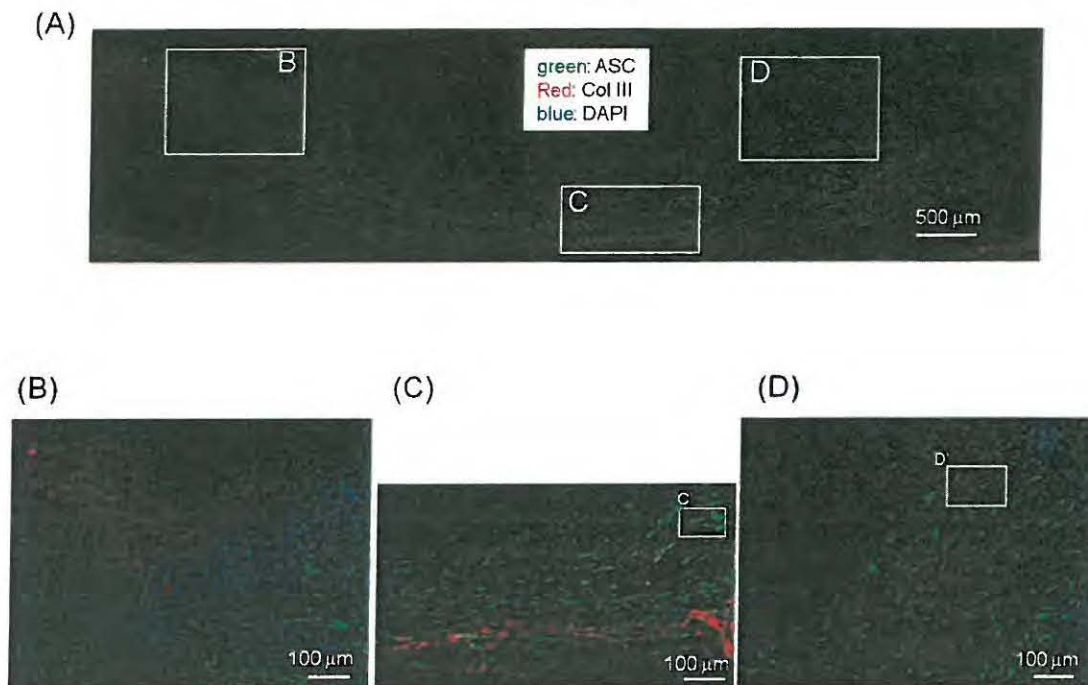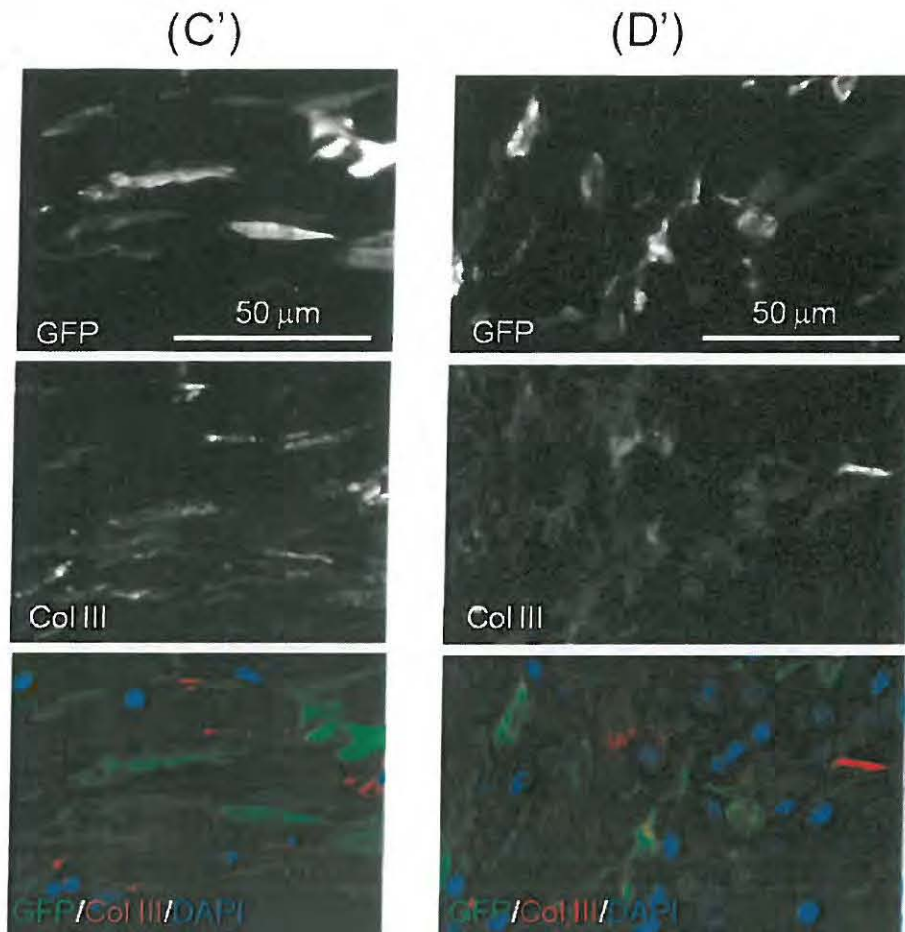
Figure 9. Expression of collagen III (Col III) in wounds. Rabbit ear wounds at POD7 were stained with chicken anti-GFP (green) and mouse anti-Col III (red) antibodies. Nuclei were stained with DAPI. (A) Low magnification of wounds. (B-D) Higher magnifications of the indicated regions (white squares) in A. (C'-D') Higher magnifications of the indicated regions in C, D. Scale bars: 500 µm (A), 100 µm (B, C, D), 50 µm (C', D').

Transdifferentiation of ASCs to endothelial cell was addressed using a platelet endothelial cell adhesion molecule (PECAM-1, CD31) - specific antibody. CD31 in blood vessels of non-wounded skin was prominently detected (data not shown). Expression of CD31 in wounds was also detected (Figure 10). However, co-expression of CD31 in transplanted ASC was not detected at POD7. Proliferation of transplanted ASCs was detected with Ki-67 or PCNA specific antibodies (Figure 11 & 12).
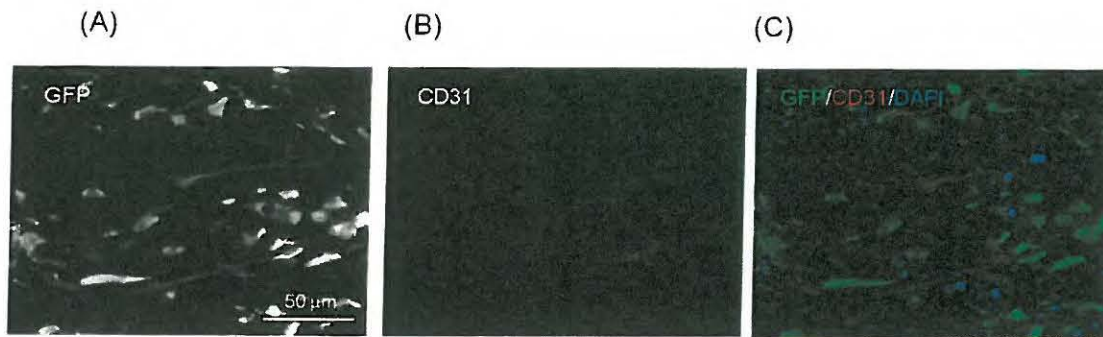
Figure 10. Expression of CD31 (PECAM-1) in transplanted ASCs. Rabbit ear wounds at POD7 were stained with chicken anti-GFP (A) and mouse anti-CD31 (B) antibodies. Nuclei were stained with DAPI. Merged image was shown in C. Scale bar; 50 μm.
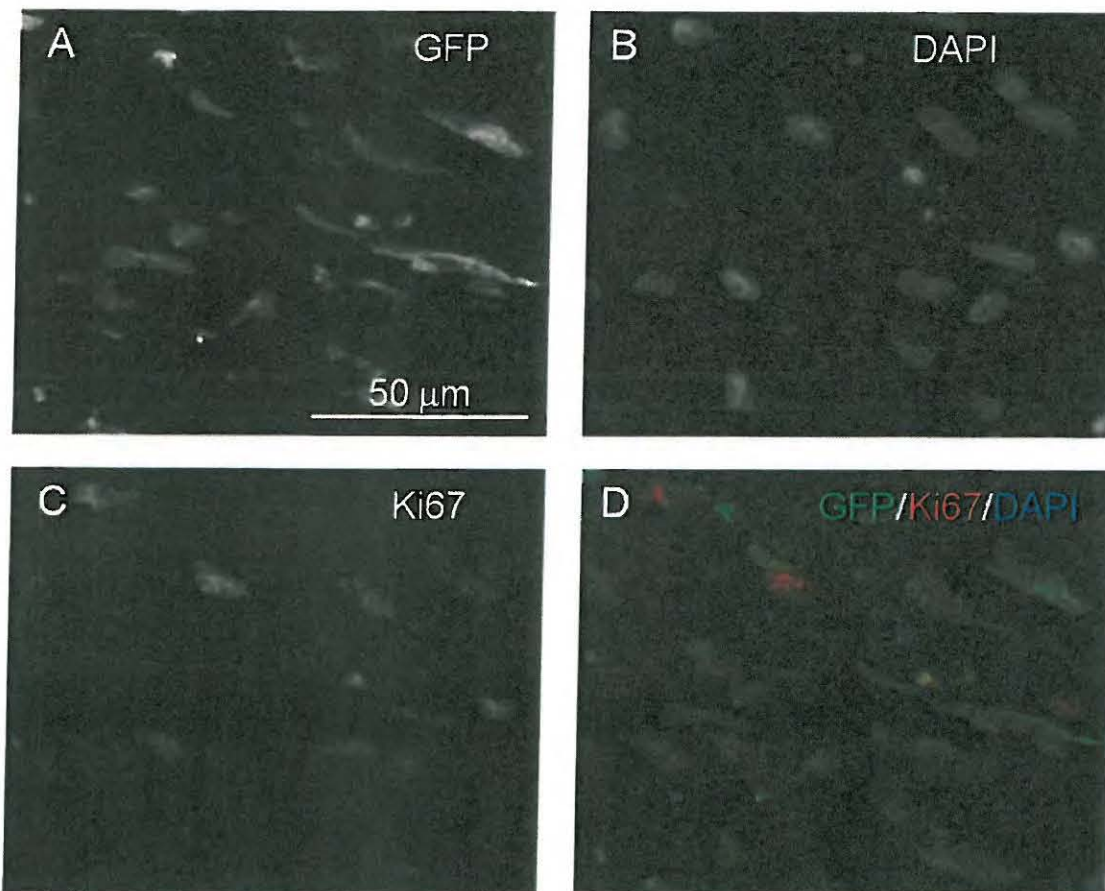
Figure 11. Proliferation of transplanted ASCs in wounds. Rabbit ear wounds at POD7 were stained with chicken anti-GFP (A) and mouse anti-Ki67 (C) antibodies. Nuclei were stained with DAPI (B). Merged image was shown in D. Scale bars: 50 μm.

10
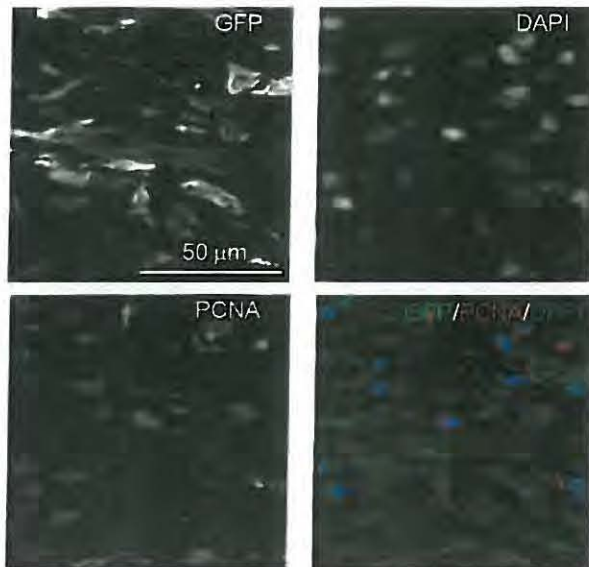
Figure 12. Transplanted ASCs proliferate in wounds. GFP-expressing ASCs were analyzed 7 days after transplanting in wounds. Chicken anti-GFP (A) and mouse anti-PCNA (C) antibodies were used. Nuclei were stained with DAPI (B). Merged image was shown in D. Scale bars: 50 μm.

3.2. ASCs enhance wound healing by increased recruitment of macrophages

We further analyzed ASCs treated- and vehicle- (saline treated-) wounds immunohistochemically. Expression of α-SMA was found in the granulation tissue of ASCs treated-wounds and saline-treated control wounds (Figure 13A & 13C). α-SMA signals in Figure 13C are from endogenous activated fibroblasts and transplanted ASCs in ASCs-treated wounds (Figure 8). α-SMA signals in Figure 13A are from endogenous activated fibroblast cells. Cells used in the transplantation are allogeneic ASCs. We investigated whether allogeneic ASCs evoke immune reaction *in vivo*, though ASCs in general possess immune modulatory properties and are not immunogenic. In this case, neither CD3 (T cell antigen) nor CD45 (common leukocyte antigen) positive signals were found in the wounds based on immunostaining using specific antibodies on treated-wounds at POD7 (Figure 13D and data not shown).

11
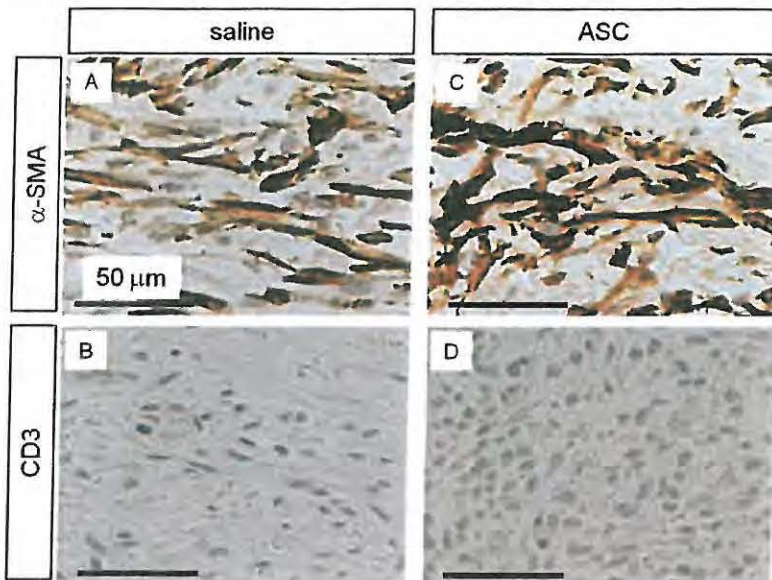
Figure 13. Analysis of rabbit activated fibroblasts and T cells in ASC-treated wounds. Saline (control; A, B) and ASCs (C, D) were delivered to wounds and harvested at POD7. α-SMA (A, C) and CD3 (B, D) were visualized by DAB after staining with their specific antibodies. Images were taken from the area labelled as 'D' in Figure 9A. Scale bars: 50 μm.

Angiogenesis is one of critical factors in wound healing process. Blood vessel formation in granulation tissue, which is determined by endothelial marker (CD31) staining, was detected in ASCs treated wounds and saline controls (Figure 14A & 14C). Interestingly, a few CD31 positive cells were found in the wound beds of ASCs-treated wounds, though blood vessel structures were not found (Figure 14D). In contrast, we were not able to detect CD31 positive cells in saline-treated wounds at POD7 (Figure 14B). Since transdifferentiation of ASCs to endothelial was not found at POD7 in our animal model (Figure 10), we speculate that these CD31+ cells were being recruited by the transplanted ASCs in wounds.
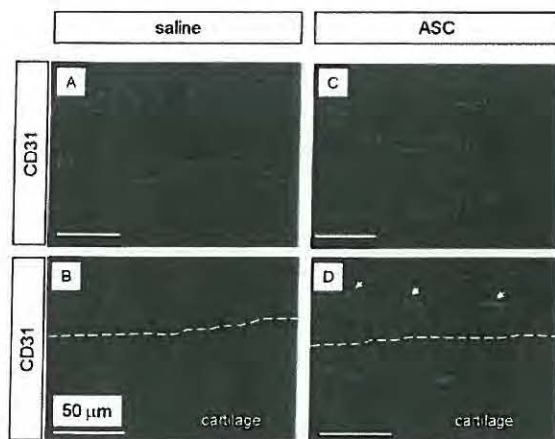
Figure 14. Analysis of CD31 in rabbit ASC-treated wounds. Saline (A, B) and ASCs (C, D) were delivered to wounds and harvested at POD7. CD31 was stained with its specific antibody and visualized using a fluorescence-conjugated secondary antibody. (A, C): images were taken from the area labelled as

12

'D' in Figure 9A. (B, D): images were taken from the area labelled as 'C' in Figure 9A. The junctional area between the cartilage and wound bed was demarcated by white dot lines. CD31 positive signals were indicated by arrows in D. Scale bars: 50 μm.

Upon tissue injury, neutrophils migrate to the wounded site and participate in the initial inflammatory phase of wound healing. Macrophages move to the site subsequently to clear the apoptotic neutrophils from the site and participate in the resolution phase of the inflammatory response and the beginning of the proliferation phase of wound healing by secreting cytokines and growth factors which attract cells such as fibroblasts that are involved in the process of wound repair, i.e., the remodelling of the extracellular matrix and the formation of granulation tissue to repair wounds. In our analysis of the treated wounds at POD7, we did not detect a significant number of neutrophils in the wounds treated with ASCs (Figure 15A & 15B). This is likely due to the fact that neutrophils arer short-lived and it is likely to be cleared by the macrophages following the initial influx of neutrophils. By contrast, we detected an average of 16.4 macrophages in the granulation tissue near the migrating epidermis in high power microscopic fields (HPF, Figure 15C & Figure 16). The number of macrophages in the granulation tissue was markedly increased by ASCs treatment at POD7 (Figure 15D & Figure 16). Thus, our wound analysis suggested that transplanted ASCs exhibit anactivated fibroblast phenotype and enhance wound repair by macrophage recruitment.
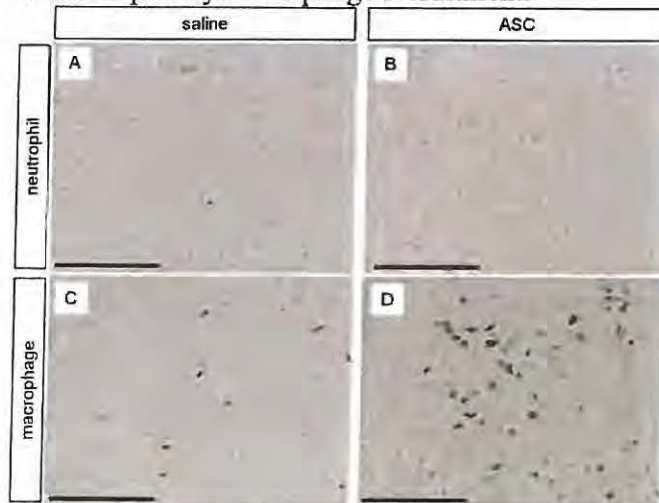
Figure 15. Detection of rabbit neutrophils and macrophages in ASC treated wounds. Saline (A, C) and ASCs (B, D) were delivered to wounds and harvested at POD7. Neutrophils (A, B) and macrophages (C, D) were visualized by DAB after staining with their specific antibodies. Scale bars: 100 μm.

13
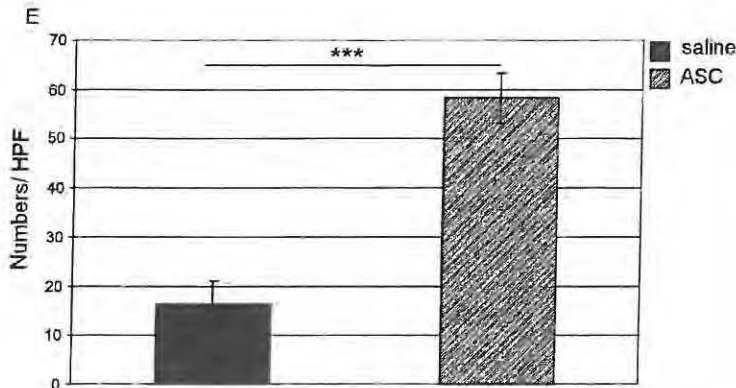
Figure 16. A higher amount of infiltration of rabbit macrophages was found in ASC-treated wounds. Macrophages per high-power microscopic field (HPF) (at 400 X magnification) were counted and averaged from four HPFs. Data are from four independent wounds and presented as mean ± SEM. ***p<0.001

II. Effect of rabbit MSCs on hypertrophic scarring

1. Effect of rabbit ASCs on hypertrophic scarring

We have determined that saline is suitable as the vehicle to deliver MSC and 1 x 10^5 of MSCs was found to be the optimum cell number for reducing hypertrophic scars in our preliminary experiments. In order to increase the statistical power of analysis for determining the quantitative differences of measurement of SEI, we increased the number of wounds and animals. P3 ASCs were harvested, washed in PBS, and resuspended in PBS. Each 7 mm wound on one of the ears of animals was treated with 1 x 10^5 ASCs in 7 µl of PBS. For wounds on the contralateral ear of the test animals, 7 µl of PBS was applied per wound to serve as the control. Wounds were harvested at POD28. There was no difference in SEI between samples treated with saline (SEI = 1.66 ± 0.07, n=33) or ASCs (SEI = 1.64 ± 0.07, n=34, p=0.82) (Figure 17A). No difference was found in scar area between the two groups (Figure 17B). Similar observations were found with the use of BM-MSCs and DFs.
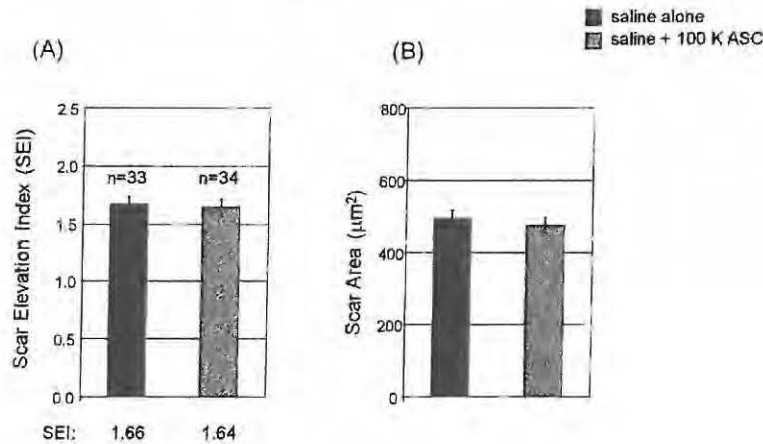
Figure 17. Histological quantification of ASCs treated scars. 1×10^5 ASCs in PBS were delivered to 7 mm wounds on one ear. In the contralateral ear, PBS alone was delivered as a control. Wounds were harvested at POD28, and SEI and scar area were measured. Data were shown as mean $\pm$ SEM.

## 2. Analysis of the quality of scars

At present, the data indicated that rabbit ASCs, rabbit BM-ASCs, and rabbit DFs did not lessen the scarring of our rabbit ear wounds. The immediate plan is to analyse the quality of scar by immunostaining using col1 and col3 specific antibodies. In addition, immature and mature collagen will be quantified using the NIH ImageJ program after Picrosirius and Masson's Trichrome staining. To examine the functional recovery of wounds by ASCs, we will determine the stress strain curves and breaking points of scars using a tensometer. At the time of preparing this Progress Report, we have transplanted 1 $\times 10^5$ ASCs wounds to wounds on one ear and saline on the contralateral ear. These wounds will be harvested on POD28 and will be analysed for scar quality as compared to PBS treated-wounds.

III. Use of other matrices as MSCs delivery vehicles to reduce hypertrophic scarring

Though we observed survival of ASCs in wounds at POD7, long-term survival of ASCs in wound (such as at POD28) has not yet been addressed. Enhanced survival of ASCs may be necessary to reduce scar formation. As we discussed in the Y1 annual report, the purity and quality of fibrinogen and thrombin are not consistent among different vendors. Thus, we tested fibrins from different vendors (e.g., Sigma-Aldrich) as a delivery vehicle. First, we treated 7 mm wounds with fibrin alone or saline alone (without ASCs), and analyzed scarring at POD28. There was no difference in SEI and scar area between samples treated with saline or fibrin (data not shown). Next, 1×10^5 P3 ASCs in a fibrin vehicle (Sigma-Aldrich) was delivered to each wound on one ear and the same quantity of ASCs in saline vehicle was delivered to wounds on the contralateral ear. Wounds which received ASCs in fibrin (n=9) showed reduction of SEI compared to wounds receiving ASCs in saline (n=7) (1.74 ± 0.08 vs 2.13 ± 0.11, respectively; $p < 0.05$) (Figure 18A). However, there was no statistical difference in scar area between the two groups (Figure 18B). These results suggest the need for optimization of MSCs delivery vehicles in order to determine the ability of ASCs to reduce scar formation. At present, we are optimizing the conditions for delivery of rabbit ASCs in fibrin.

15
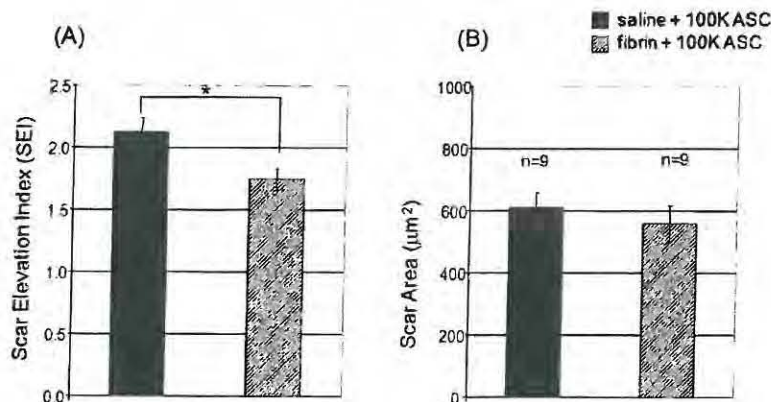
Figure 18. Histological quantification of ASCs-treated scars. 1×10^5 ASCs in Sigma-Aldrich fibrin or saline were delivered to the wounds. Wounds were harvested at POD28, and SEI and scar area were measured. Data are shown as mean $\pm$ SEM. *p<0.05.

IV. Comparison of allogeneic and autologous ASCs in stem cell therapy.

Alllogeneic ASCs have been used in our wound healing and scarring experiments as described above. We were interested in determining whether allogeneic ASCs have a similar ability, as compared to autologous ASCs, in promoting wound healing and reducing scarring. In this case, autologous ASCs were isolated from one of the inguinal fat pads and cultured *in vitro* prior to the application of the cells to the wounds of the animal (Figure 19).
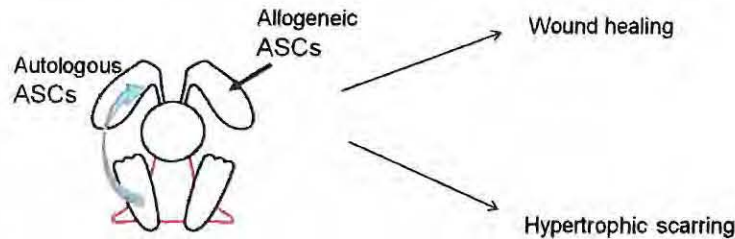
Figure 19. Schematic drawing of autologous and allogeneic ASC treatments in rabbits.

Once rabbits were fully recovered from surgery, P1 allogeneic or autologous ASCs (1×10^5) in 7 µl of PBS were delivered to each 7 mm wound on one ear or the contralateral ear respectively. Wounds were harvested at POD7, 14, 28. Analysis of wounds at POD7 showed that there were no significant differences in wound healing parameters between the two test groups with regard to the epithelial gap ($3,443 \pm 524$ µm vs. $2,702 \pm 589$ µm, autologous vs. allogeneic, respectively; p =0.6), granulation tissue distance ($1,169 \pm 67$ µm vs. $1,135 \pm 75$ µm, respectively, p=0.37), and granulation tissue area ($572,146 \pm 68,226$ µm^2 vs. $612,048 \pm 46,521$ µm^2; p =0.49) (Figure 20).
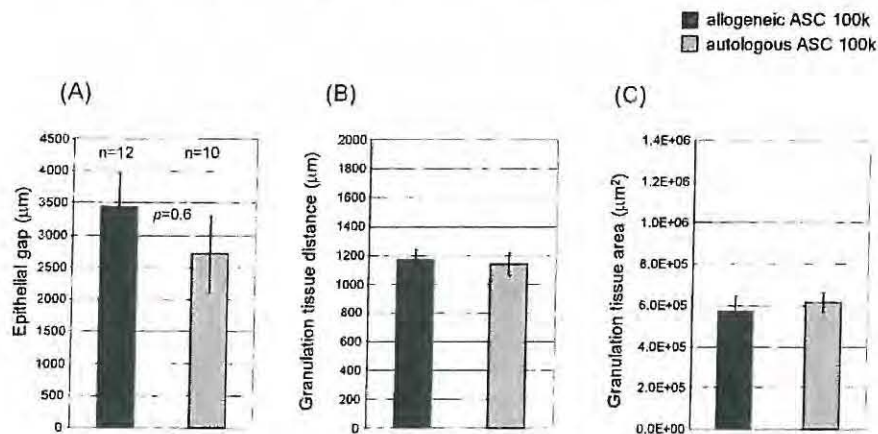
Figure 20. Histological quantification of wounds treated with allogeneic and autologous ASCs. P1 allogeneic or autologous ASCs (1×10^5) in 7 µl of PBS were delivered to each 7 mm wound on one ear or the contralateral ear. Wounds were harvested at POD7 and epithelial gap (A), granulation tissue distance (B), and granulation tissue area (C) were measured. Data shown as mean $\pm$ SEM.

Scar analysis at POD28 showed no difference of SEI in wounds where allogeneic (SEI = 1.31 $\pm$ 0.09, n=11) or autologous (SEI = 1.33 $\pm$ 0.1, n=12, p=0.79) ASCs were transplanted (Figure 21A). No difference was found in scar area between the two groups (Figure 21B). We further analyzed for the presence of CD3 and CD45 marker cells in wounds treated with allogeneic or autologous ASCs to determine the occurence of any immune reactions. Neither CD3 nor CD45 positive signals were found in these treated wounds at POD7, 14, and 28 using specific antibodies against these markers (data not shown). The results suggest that allogeneic ASCs do not have any excessive immune response and therefore could potentially be used in cell therapy.

■ allogeneic ASC 100k
▓ autologous ASC 100k
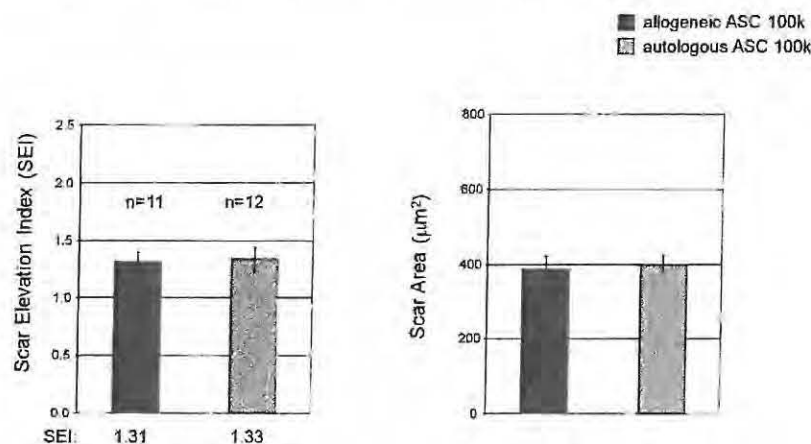
Figure 21. Histological quantification of allogeneic and autologous ASCs treated scars. P1 allogeneic or autologous ASCs (1×10^5) in 7 µl of PBS were delivered to each 7 mm wound on one ear or the contralateral ear. Wounds were harvested at POD28, and SEI and scar area were measured. Data shown as mean $\pm$ SEM.

V. *In Vitro* Characterization of Rabbit Mesenchymal Stem Cells (MSC) Aggregates

1. Synthesis and Culture of Rabbit MSC Aggregates

One of our objectives in the proposed study is to understand the paracrine profile of rabbit ASCs grown 2-dimensionally (2-D) versus 3-dimensionally (3-D). We have successfully generated scaffold-free, size-controlled cell aggregates via a forced aggregation technique using micropatterned wells (AggreWellTM, STEMCELL Technologies) originally developed for embryonic stem cells (ESC)/ induced pluripotent stem cells (iPS) research. We were capable of producing cell aggregates of different sizes ranging from 125 cells per aggregate to 16,000 cells per aggregate.
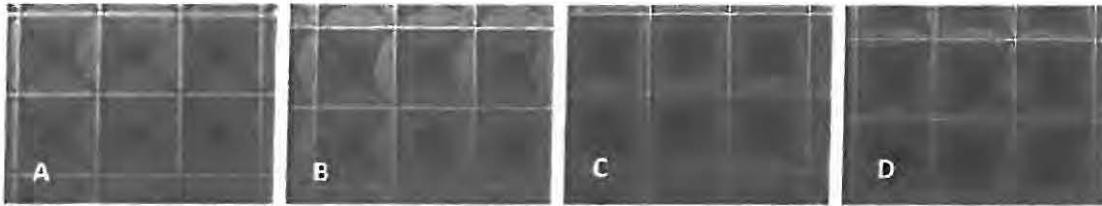
Figure 22: Phase-contrast images of rabbit ASCs seeded in micropatterned wells at different cell densities. 250 cells per aggregate (A), 500 cells per aggregate (B), 1000 cells per aggregate, and 2000 cells per aggregate. These images were taken right after plating and centrifugation. Magnification, ×50.

Figure 22 (a-d) are phase-contrast images of rabbit adipose-derived stem cells (ASCs) at four different seeding densities (250 cells/aggregate, 500 cells/aggregate, 1000 cells/aggregate, and 2000 cells/aggregate) right after plating and centrifugation. ASCs compacted to form self-assembling cell aggregates after overnight incubation (as shown in Figure 23). ASC aggregates can be cultured in micropatterned wells for extended periods of time without loss of cell viability. They can also be harvested from micopatterned wells and cultured in suspension.
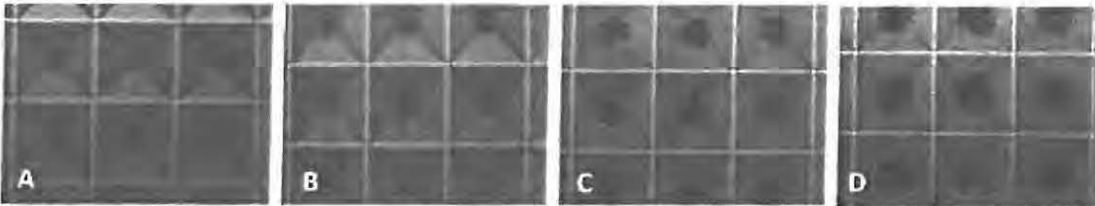
Figure 23: Rabbit ASCs compacted to form cell aggregates overnight.. (A) 250 cells per aggregate, (B) 500 cells per aggregate, (C) 1000 cells per aggregate, and (D) 2000 cells per aggregate. Magnification, ×50.

2. Gene Expression and Protein Expression of MSCs as 3D Aggregates vs. Adherent Monolayers

We have examined the expression of a selected panel of genes pertinent to wound healing in rabbit MSCs cultured under 3D vs. 2D conditions. An up-regulation of markers linked to angiogenesis such as vascular endothelial growth factor A (VEGFA), fibroblast growth factor 2 (FGF2), and hepatocyte growth factor (HGF) was observed in 3D aggregates of rabbit dermal fibroblasts (DFs), adipose-derived stem cells (ASCs), and bone marrow-derived stromal cells (BMSCs). An up-regulation of keratinocyte growth factor (KGF) and transforming growth factor β-1 (TGFβ-1) was also observed in all cell types cultured under 3D conditions, whereas a down-regulation of factors connective tissue growth factor (CTGF), epithelial growth factor (EGF), transforming growth factor β-2 (TGFβ-2) was observed. Most interestingly, transforming growth factor β-3 (TGFβ-3) was down-regulated in rabbit DFs and BMSCs, but was up-regulated in rabbit ASCs. TGFβ-3 has been implicated in reducing scarring in wounds. A summary of the gene expression data is depicted in Table 1.

18

Table 1: Summary of the changes in gene expression in rabbit DFs, ASCs, and BMSCs cultured under3D vs. 2D conditions.

	VEGFA	FGF2	HGF	KGF	EGF	CTGF	TGFβ$_1$	TGFβ$_2$	TGFβ$_3$
Rb DF	↑	↑	↑	↑	↓	↓	↑	↓	↓
Rb ASC	↑	↑	↑	↑	↓	↓	↑	↓	↑
Rb BMSC	↑	↑	↑	↑	↓	↓	↑	↓	↓

We have also confirmed the secreted protein expression of a few key factors. Due to the lack of commercially available rabbit reagents, we were constrained to human specific assays that have reported cross-reactivity with the rabbit. Some of these factors included VEGF, FGF2, TGFβ-1, and TGFβ-2. Our immunoassay data showed excellent correspondence with our gene expression findings.

Future work will focus on an extended list of genes from the wound healing, fibrosis, and inflammation panels via the use of a customized, high-throughput PCR Array technology (RT^{2}Profiler^{TM} PCR Array, QIAGEN), where we can screen up to 84 genes per panel.

KEY RESEARCH ACCOMPLISHMENTS IN YEAR 2.

A. Wound healing study
- Optimized the cell number of rabbit ASCs (1 x 10^6 ASCs per 7 mm wound) for wound healing study.
- Completed histological analyses on the effects of ASCs, BM-MSCs, and DFs on wound healing.
- Demonstrated that rabbit ASCs promoted granulation tissue formation.
- Completed histological analysis of growth-arrested ASCs treated wounds and demonstrated that these MitC-treated cells did not any effect on wound healing.
- Determined that Transplanted ASCs exhibited the activated a phenotype.
- Determined that transplanted ASCs can proliferate in wounds.
- Demonstrated that ASCs enhanced wound healing by increased recruitment of macrophages.
- Preparation of a manuscript.

B. Hypertrophic scar study
- Optimized the cell number (1 x 10^6 ASCs per 7mm wound) for hypertrophic scar study.
- Completed histological analyses on the effect of treatments by ASCs, BM-MSCs, and DF in reducing hypertrophic scarring.

- Demonstrated that none of the cell treatments tested reduced scarring.
- In the process of harvesting scars for the collagen analysis by immunostaining, Picrosirus staining, and Masson's Trichrome staining.
- In the process of determining the tensile strength of hypertrophic scars from wounds treated with rabbit ASCs as compared to that of controls.
- Determined that allogeneic ASCs could be used as cell therapy.

C. 3-D cell aggregate study
- As compared to 2-D cultures, 3-D ASCs showed an up-regulation of growth factors that include KGF, TGFβ-1, VEGF, FGF2, HGF, and TGFβ-3 at mRNA transcript levels and at protein levels with some of these factors(VEGF, TGFβ1 &2, and FGF2) .

REPORTABLE OUTCOMES

A. Wound healing study
  (1) Demonstrated that rabbit ASCs promoted granulation tissue formation.
  (2) Determined that Transplanted ASCs exhibited the activated fibroblast phenotype.
  (3) Determined that transplanted ASCs can proliferate in wounds.
  (4) Demonstrated that ASCs enhanced wound healing by increased recruitment of macrophages.
  (5) Preparation of a manuscript.

B. Hypertrophic scar study
  (1) Demonstrated that none of the cell treatments tested reduced scarring.
  (2) Determined that allogeneic ASCs could be used as cell therapy without inducing immunological responses.

C. 3-D cell aggregate study
  (1) As compared to 2-D cultures, 3-D ASCs showed an up-regulation of growth factors that include KGF, TGFβ-1, VEGF, FGF2, HGF, and TGFβ-3 at mRNA transcript levels and at protein levels with some of these factors(VEGF, TGFβ1 &2, and FGF2) .
  (D) Immediate future plan
  (1) In the process of harvesting scars for the collagen analysis by immunostaining, Picrosirus staining, and Masson's Trichrome staining.
  (2) In the process of determining the tensile strength of hypertrophic scars from wounds treated with rabbit ASCs as compared to that of controls.
  (3) Test the 3D grown rabbit ASC in reducing hypertrophic scarring in our rabbit ear hypertrophic scar model

CONCLUSION

Topically delivered 2-dimensionally grown rabbit ASC (2D ASC) increased granulation tissue formation in wounds without affecting epithelialization when compared to saline control. Transplanted 2D rabbit ASC exhibited activated fibroblast phenotype and enhanced macrophage recruitment in wounds. However, 2-D rabbit ASC had no effect on hypertrophic scarring. Scar analysis at POD28 showed no difference on Scar Elevation Index in wounds where allogeneic (SEI = 1.31 + 0.09, n=11) or autologous (SEI = 1.33 + 0.1, n=12, p=0.79) ASCs were transplanted. One of our objectives in the proposed study was to understand the paracrine profile of rabbit ASCs grown 2-dimensionally versus 3-dimensionally (3D). We have successfully generated scaffold-free, size-controlled cell aggregates (3D cell culture) via a forced aggregation technique using micropatterned wells. An up-regulation of markers linked to angiogenesis such as vascular endothelial growth factor A (VEGFA), fibroblast growth factor 2 (FGF2), and hepatocyte growth factor (HGF) was observed in 3D aggregates of rabbit dermal fibroblasts (DFs), ASCs, and bone marrow-derived stromal cells (BMSCs). An up-regulation of keratinocyte growth factor (KGF) and transforming growth factor β-1 (TGFβ-1) was also observed in all cell types cultured under 3D conditions, whereas a down-regulation of factors such as connective tissue growth factor (CTGF), epithelial growth factor (EGF), transforming growth factor β-2 (TGFβ-2) was observed. Most interestingly, transforming growth factor β-3 (TGFβ-3) was down-regulated in rabbit DFs and BMSCs, but was up-regulated in rabbit ASCs. TGFβ-3 has been implicated in reducing scarring in wounds. The up-regulation of some of these growth factors (VEGF, TGFβ1 &2, and FGF2) also occurred at protein levels. Future work will focus on an extended list of genes from the wound healing, fibrosis, and inflammation panels via the use of a customized, high-throughput PCR Array technology (RT2ProfilerTM PCR Array, QIAGEN), where we can screen up to 84 genes per panel. Additionally, because of the up-regulation (as compared to the 2D counterpart) of the 3D ASC in producing growth factors essential in wound healing and the down-regulation of scar-promoting factor such as CTGF, we will test the 3D grown rabbit ASC in reducing hypertrophic scarring in our rabbit ear hypertrophic scar model.

REFERENCES

None

APPENDICES

None

Superiority of adipose derived stem cell over bone-marrow derived mesenchymal stem cell and dermal fibroblast in wound healing.

Seok Jong Hong[a], Sheng-Xian Jia[a], Ping Xie[a], Wei Xu[a], Kai P. Leung[b], Thomas A. Mustoe[a], Robert D. Galiano[a]

[a]Laboratory for Wound Repair and Regenerative Medicine

Department of Surgery/Division of Plastic and Reconstructive Surgery

Northwestern University, Feinberg School of Medicine

[b]Microbiology Branch, US Army Dental and Trauma Research Detachment, Institute of Surgical Research, Fort Sam Houston, Texas

S.X.J. and P.X. contributed equally to this article.

Short running title: ASC in wound healing

Key words: Adipose derived stem cells (ASC), wound healing, multipotency, rabbit ear model, activated fibroblast, macrophages

Correspondence:

email: Seok Jong Hong (seok-hong@northwestern.edu) *or* Robert D. Galiano (rgaliano@nmh.org)

ABSTRACT

Multipotent mesenchymal stem cells (MSC) are found in various tissues and can proliferate extensively *in vitro*. MSC have been used in preclinical animal studies and clinical trials in many fields. Adipose derived stem cells (ASC) have several advantages compared to other MSC for use in cell-based treatments because they are easy to isolate with relatively abundance. However, quantitative approaches for wound repair using ASC have been limited because of lack of animal models which allow for quantification. Here, we addressed the effect of topically delivered ASC in wound repair by quantitative analysis using the rabbit ear model. We characterized rabbit ASC, and analyzed their multipotency in comparison to bone marrow derived-MSC (BM-MSC) and dermal fibroblast (DF) *in vitro*. Topically delivered ASC, not BM-MSC or DF, increased granulation tissue formation in wounds when compared to saline control. Our *in vitro* and *in vivo* studies suggest that ASC and BM-MSC are not identical, though they have similar surface markers. We found that topically delivered ASC are engrafted and proliferate in the wounds. We showed that transplanted ASC exhibited activated fibroblast phenotype and enhanced macrophage recruitment *in vivo*.

INTRODUCTION

Wound repair is a complex and dynamic process which consists of inflammation, angiogenesis, and tissue formation and remodeling [1-3]. Upon injury, fibrin clots are deposited on the wound site to prevent hemorrhage. Circulating platelets migrate to the wound and release inflammatory signals such as transforming growth factor-β (TGF-β), platelet-derived growth factor (PDGF), and epidermal growth factor (EGF). This is

followed by the infiltration of neutrophils and macrophages and the migration of keratinocytes to the wound to recover the barrier function of skin. Endothelial cells and fibroblasts migrate to the site and build up granulation tissues by depositing collagen and other extracellular matrices. During the final stages of repair, fibroblasts remodel the collagen by producing matrix metalloproteinases (MMPs) over a course of several months. Thus wound repair is a highly orchestrated sequential process in which signals of one cell type regulate other cell types in a cascade.

Growth factors have been used to improve the clinical outcome of the wound repair process. It has become clear that the use of growth factors, specifically as single-agent therapies, has limited impact on wound repair [4]. This could be partly due to the rapid degradation of therapeutic growth factors in the wound site or the requirement for the administration of these growth factors in a proper spatiotemporal sequence in order to improve wound repair. Recent progress in regenerative medicine has suggested multipotent stem cells or progenitor cells for tissue repair [4, 5]. It is thought that the transplanted stem cells or progenitor cells can integrate themselves to the environment and control the wound repair process by secreting factors and communicating with other cells to improve the clinical outcome of wound repair. In addition, stem cells could mediate wound repair by replacing damaged tissue by both differentiating into the required cells and inducing surrounding cells to dedifferentiate to replace the tissues.

MSC have been found from various tissues such as bone marrow, adipose tissue, umbilical cord blood, skeletal muscle, and brain [6, 7]. MSC have ability to attach to plastic to form fibroblast-like colonies and to proliferate extensively *in vitro*. MSC can be differentiated into multiple lineage cells: chondrocytes, cardiomyocytes, adipocytes,

osteoblasts, endothelial, and neuronal cells [7-10]. Among MSC, ASC can be easily obtained with large quantities as well as minimal morbidity and invasion [11-13]. ASC activate repair processes in a paracrine manner by secreting cytokines and growth factors, such as vascular endothelial growth factor (VEGF), TGF-β, granulocyte/ macrophage colony stimulating factor (GM-CSF), stromal derived factor 1 (SDF-1), and hepatocyte growth factor (HGF) [14]. These cells also recruit endogenous stem (or progenitor) cells and can stimulate them to differentiate into the required cell types. ASC suppress immune reactions and have reduced histocompatability antigens [15-17]. ASC have been used in preclinical animals studies and clinical trials in the field of reconstructive surgery, orthopedics, and immune diseases [7, 12, 18, 19].

Many animals - such as mouse, rat, rabbits, and pigs - have been used in wound healing studies. However, there is no perfect model which exactly resembles human wounds. For example, open wounds in rodents heal quickly. This is accomplished almost entirely by wound contraction because of the subcutaneous panniculus carnosus muscle. This is in marked contrast to human skin wounds which heal to a significant degree by generation of new tissue (granulation tissue and re-epithelialization). Thus, though ASC are a promising candidate for cell therapy in wound repair, there have been limitations in the quantitative analysis of wound repair [20-22]. The rabbit ear model has a unique advantage in wound healing study because of the ability to evaluate the role of therapeutic treatment in wounds by quantification of epithelialization and granulation tissue formation [23-25]. In this report, we addressed the effect of topically delivered ASC in wound repair by quantitative analysis using the rabbit ear model. We characterized rabbit ASC, and analyzed their multipotency in comparison to BM-MSC

and DF *in vitro*. In addition, the effect of wound healing by ASC treatment was compared to BM-MSC and DF treatment. Wound analysis suggests that topically delivered ASC exhibit activated fibroblast phenotype, enhance macrophage recruitment, and increase granulation tissue formation in wounds.

MATERIALS AND METHODS

Isolation and culture of ASC, BM-MSC, and DF

ASC were isolated as described previously with some modification [9, 24]. Briefly, inguinal fat pads were dissected out from young female New Zealand White rabbits (3-6 months old, ~2-4 kg) and placed in sterile, pre-warmed phosphate-buffered saline (PBS). Fat pads were then washed several times in PBS, minced manually, and digested in 0.075% collagenase type II in Hank's Buffered Salt Solution (HBSS) for 1 hour at 37°C in a shaking water bath. The stromal vascular fraction (SVF) containing ASC was isolated by centrifugation at 500 x g for 5 minutes, resuspended in HBSS, filtered through a 100 μm sterile nylon mesh filter, and then spun again at 500 x g for 5 minutes. The resultant pellet was resuspended in 10 ml of red blood cell (RBC) lysis buffer (10 mM $KHCO_3$, 150 mM NH_4Cl, 0.1 mM EDTA), and allowed to sit at room temperature for 10 minutes. The supernatant was removed by centrifugation following RBC lysis and the pellet was resuspended in Dulbecco's Modified Eagle Medium: Nutrient Mixture F-12 (DMEM/F12) containing 10% fetal bovine serum (FBS, Thermo Scientific, Rockford, IL) and plated in culture dishes. After overnight culture, the media was then removed and

replaced with fresh culture medium. The medium was changed twice a week and ASC were subcultured when they reached 80-90% confluency.

BM-MSC were isolated from the femoral medullary cavities of rabbits. Bone marrow was collected in PBS containing 2 units/ml heparin and left at room temperature for 10 minutes. After removing the floating fat layer, the solution was added to 5 ml of Ficoll-Paque Plus (1.077 g/ml, GE Healthcare, Piscataway, NJ) in a 15 ml tube and centrifuged at 2,000 x g for 30 minutes. The interface layer containing BM-MSC was recovered and washed in HBSS. BM-MSC were then cultured in Minimum Essential Medium (MEM) containing 10% FBS.

For the isolation of rabbit dermal fibroblasts (DF), skin tissue was cut into squared pieces (~ 1 x 1 cm^2) and placed with the epidermis face down in a dish. Dispase (Life Technologies, Carlsbad, CA) with 5 mg/ml in PBS was added and incubated overnight at 4°C. Dermal tissue was minced manually after removing epidermal tissue and digested in 0.25% collagenase type II (Life Technologies) in HBSS at 37°C overnight. The solution was filtered through a 100 µm sterile nylon mesh filter and spun at 500 x g for 10 minutes. The pellet was then resuspended in DMEM medium containing 10% FBS and cultured in culture dishes.

In vitro differentiation of MSC to mesodermal lineage

For adipogenic differentiation, MSC were seeded in 24 well plates at a concentration of 2 x 10^4 and cultured in adipogenesis differentiation medium (Life Technologies). After 8 days culturing, cells were fixed in 4% paraformaldehyde and Oil Red O staining was performed to detect intracellular lipid accumulation. For osteogenic differentiation, MSC

were seeded in collagen (50 µg/ml) coated 24 well plates at a concentration of 1×10^4 and cultured in osteogenesis differentiation medium (Life Technologies) for 28 or 35 days. Cells were fixed in 4% paraformaldehyde and Alizarin Red S staining was performed to detect accumulated calcium. For chondrogenic differentiation, a total of 8×10^4 MSC in 20 µl of culture medium were plated in the middle of 24 well plate. After 3 hours incubation, chondrogenesis differentiation medium was provided (Life Technologies). After 14 or 21 days of culture, cells were fixed in 4% paraformaldehyde. Then, Alician Blue Staining was performed, which detected sulfated proteoglycan rich matrix.

Reverse transcription-quantitative PCR (RT-qPCR) and Western blot analysis

Total RNA was prepared by treatment with Trizol Reagent (Sigma-Aldrich, St. Louis, MO) and genomic DNA was removed using the Turbo DNA-free kit (Ambion, Austin, TX). cDNA was made from total RNA using superscript II (Invitrogen, Carlsbad, CA) with random primers. PCR was performed to detect expression of mRNAs. For the quantitative analysis, RT-qPCR analyses using SYBR green I were performed using an ABI prism 7000 sequence detection system (Applied Biosystems, Foster City, CA). Expression of each gene was normalized to the level of glyceraldehyde-3-phosphate dehydrogenase (Gapdh) to get a ΔCt. The $2^{-\Delta\Delta Ct}$ method was used to calculate gene expression difference between differentiated and control samples. Expression of genes was detected by PCR with the following oligonucleotides – Gapdh (5'-AGGTCATCCACGACCACTTC -3' and 5'- GTGAGTTTCCCGTTCAGCTC -3'),

adiponectin (5'- CCTGGTGAGAAGGGTGAAAA -3' and 5'-

GCTGAGCGGTAGACATAGGC -3'), osteopontin (5'-

AGGATGAGGACGATGACCAC -3' and 5'- CACGGCCGTCGTATATTTCT -3'),

col10a1 (5'- GGAAAACAAGGGGAGAGAGG -3' and 5'-

CCAGGAGCACCATATCCTGT -3').

For Western blot analysis, MSC were washed with PBS, harvested, and lysed

with RIPA buffer (150 mM NaCl, 1% NP-40, 0.5% deoxycholic acid, 0.1% SDS, 50 mM

Tris-Cl, pH 7.5). Equal amounts of protein were added to a SDS polyacrylamide gel and

transblotted on nitrocellulose membranes. Membranes were incubated with anti-CD29

(1:5,000 dilution; Abcam, Cambridge, MA), anti-CD44 (1:5,000 dilution; Abcam), anti-

CD90 (1:5,000 dilution; Abcam), or anti-CD105 (1:2,500 dilution, Abcam) and then

incubated with horseradish peroxide-conjugated secondary antibody (1:5,000 dilution;

Vector Laboratories, Burlingame, CA). Specific bands were visualized using an

Enhanced Chemiluminescence (ECL) detection kit (GE Healthcare). The blots were

probed with anti-β-actin antibody (1:5,000 dilution; Sigma–Aldrich) to serve as a control

for gel loading.

Labeling of ASC with green fluorescence protein (GFP)

To stably express GFP, ASC were transduced with a lentivirus (LV-GFP) in which GFP

expression is driven by a cytomegalovirus (CMV) promoter according to the

manufacturer's protocol (Life Technologies). Briefly, 2 multiplicity of infection (MOI) of

lentivirus was infected to ASC in the presence of 6 μg/ml of polybrene. Transduced cells

were selected by treating 10 μg/ml of blasticidin. GFP expressing cells were further selected by flow cytometry using the Northwestern University Flow Cytometry Facility.

Treatment of MSC to the full thickness excisional wounds of rabbit ears

Young, adult New Zealand White rabbits (3-6 months, ~2-4 kg) were acclimated to standard housing and fed *ad libitum* under an experimental protocol approved by the Northwestern University Animal Care and Use Committee. Rabbits were anesthetized with an intramuscular injection of ketamine and xylazine as described [24, 25]. Wounds were made with a 7 mm surgical punch biopsy (Acuderm, Ft. Lauderdale, FL) down to, but not through, the cartilage. Six wounds were created per ear. Tissue was then elevated in an effort to remove epidermis and dermis, but leave the perichondrium intact. MSC were topically delivered to wounds and wounds were then covered with semi-occlusive dressings (Tegaderm[TM], 3M Health Care, St. Paul, MN). MSC were also delivered to wounds in the fibrin gel delivery matrix in some experiments as described in the previous works [24, 25]. Wounds were harvested with a 10 mm surgical punch biopsy tool (Acuderm) at post-operative day (POD) 7 after euthanization with the administration of intracardiac Euthasol followed by a bilateral thoracotomy. Wounds were immersed in 10% zinc-formalin for fixation.

Histological and immunochemical analysis of wounds

Formalin-fixed wounds were processed, embedded in paraffin blocks, and then sectioned on a microtome at a thickness of 4 μm. The sections were stained with hematoxylin and eosin (H&E) and histological analysis - epithelial gap, new granulation tissue distance,

and granulation area - was performed using a Nikon Eclipse 50i light microscope and NIS Elements BR software (Nikon, Melville, NY) (Supporting Information Fig. S7). Slides were analyzed and scored in a blinded fashion and statistical comparisons were made with the Student's t test using a significance level of $p < 0.05$.

For the immunostaining, sections were treated with antigen retrieval solution (Dako, Carpinteria, CA) by boiling for 20 minutes before antibody treatment. For immunohistochemistry (IHC), the signal was detected using the Vectastain kit (Vector laboratories, Burlingame, CA) after primary antibody treatment and visualized using 3,3'-diaminobenzidine (DAB). Hematoxylin was used as a counterstain. Mouse anti- alpha smooth muscle actin (α-SMA, 1:2,000 dilution, Santa Cruz Biotechnology, Santa Cruz, CA), mouse anti- neutrophil Marker (RPN3/57, 1:1,000 dilution, Santa Cruz Biotechnology), mouse anti-CD3 (1:1,000 dilution, Santa Cruz Biotechnology), and mouse anti-macrophage (1:1,000 dilution, Abcam) were used as primary antibodies.

For immunofluorescence microscopy, chicken anti-GFP (1: 200 dilution, Life Technologies), α-SMA (1:200 dilution, Santa Cruz Biotechnology), mouse anti-collagen III (col3, 1:200 dilution, Novus Biologicals, Littleton, CO), mouse anti-CD31 (1:25 dilution, Abcam), mouse anti-Ki67 (1:20 dilution, Novocastra, Buffalo Grove, IL), and mouse anti-PCNA (1:100 dilution, BD Biosciences, San Jose, CA) antibodies were used as primary antibodies. Alexa Fluor 488 or 555 conjugated secondary antibodies were used to detect the primary antibody (Invitrogen). Nuclei were stained with 4',6-diamidino-2-phenylindole (DAPI, 1 μg/ml).

RESULTS

Isolation and characterization of rabbit ASC

Rabbit ASC have spindle shapes during *in vitro* primary culture and are morphologically similar to DF (Fig. 1A & 1C). Rabbit BM-MSC have a larger surface area compared to ASC (Fig. 1B). We characterized ASC by analyzing surface markers and multipotency of differentiation. Unlike embryonic stem cells, which have specific makers such as Oct-4 and SSEA, MSC can not be characterized by specific markers because definitive cellular markers are not yet identified. Thus, a series of positive and negative surface markers are needed for the characterization of MSC [6, 7, 12, 13, 19]. We selected CD29, CD44, CD 90, and CD105 as positive markers. Two hematopoietic cell markers, CD34 and CD45, were used as negative markers. Given the limited information of antibodies in rabbit protein, we tested antibodies that were designed to detect human antigens. Specificity of antibodies, except CD45, was confirmed by Western blot analysis (data not shown). Expression of CD34 was detected in neither ASC nor BM-MSC (data not shown). We tested antibodies from four different vendors but could not find antibodies which are specific to rabbit CD45 protein (data not shown). Expression of CD29, CD44, CD90, and CD105 was detected without significant changes from passage 1 through passage 9 both in ASC (Fig. 1D) and BM-MSC (Supporting Information Fig. S1).

Multi-lineage differentiation potential of ASC

MSC have the ability to differentiate into mesodermal cells such as adipocytes, chondrocytes, osteocytes, and myocytes in response to appropriate intrinsic or extrinsic

signalings [9, 13]. We addressed the multipotency of ASC, and compared them to BM-MSC and DF. For adipogeneis, Oil Red O staining showed an accumulation of lipid droplets in the cytoplasm of ASC and BM-MSC which were grown in adipogenesis medium for 8 days (Fig. 2A & B). In contrast, fewer lipid droplets were found in the cytoplasm of DF (Fig. 2C). Alician Blue staining showed positive signals in ASC and BM-MSC which were cultured in chondrogensis medium for 14 days and signals were strengthened at day 21 culture (Fig. 2D & E). Alician Blue staining positive signals were found in DF culture, though those signals were weaker compared to ASC and BM-MSC (Fig. 2F). Analysis of osteogenesis by Alizarin Red S staining showed clear staining in ASC and BM-MSC but not in DF at day 28 culture in the osteogenesis medium (data not shown). Both ASC and BM-MSC showed a high accumulation of calcium at day 35 culture (Fig. 2G & H). DF also showed an accumulation of calcium, although it was a smaller amount compared to ASC and BM-MSC in the day 35 culture (Fig. 2I).

We analyzed the expression of specific genes of adipocyte, osteocyte, and chondrocyte lineages by RT-qPCR [9]. Expression of an adipocyte specific gene, adiponectin, was increased by 35-fold and 17-fold in ASC and BM-MSC when cultured in adipogenic medium for 8 days (Supporting Information Fig. S2A). However, induction of adiponectin in DF was not found in the same culture condition. Expression of an osteocyte specific gene, osteopontin, was increased by 3.2-fold and 2.7-fold in ASC and BM-MSC respectively. This increase in gene expression was not found in DF when it was cultured in osteogenic medium for 28 days (Supporting Information Fig. S2B). Expression of a chondrocyte specific gene, Col10a1, was increased by 6-fold, 12-fold, and 1,515-fold in DF, ASC, and BM-MSC respectively, when cultured in chondrogenic

medium for 21 days (Supporting Information Fig. S2C). These results suggest that ASC and BM-MSC have differential properties, though they share similar surface markers and have multilineage differentiation potential. ASC and BM-MSC are prone to differentiate into adipocytes and chondrocytes, respectively. DF have less multipotency compared to ASC and BM-MSC.

Transplanted ASC exhibit activated fibroblast phenotype

Wound healing is a complex process in which interactions of diverse cell types and cytokines are involved. ASC can contribute to wound healing by either cytokine expression, or differentiation and repopulation in wounds. We analyzed the transplanted ASC in wounds using GFP-expressing ASC (GFP-ASC). A total of 1×10^5 GFP-ASC in saline was delivered into each wound. Wounds were harvested at POD7 and histological analysis was performed. Immunofluorescence staining with anti-GFP antibody showed that transplanted ASC were evenly distributed in the wound bed and granulation area (Fig. 3A & Supporting Information Fig. S4A). During the wound repair process, fibroblasts migrate to the wound site and build up granulation tissue by depositing collagen and other extracellular matrices [26, 27]. These activated myofibroblasts are characterized by α-SMA expression. Immunofluorescence staining with anti-α-SMA antibody detected endogenously activated fibroblasts (cells with red color, Fig. 3 & Supporting Information Fig. S3). Interestingly, the majority of transplanted ASC showed α-SMA signal (cells with yellow color, Fig. 3C, D, F, G & Supporting Information Fig. S3). We also observed ASC which did not express α-SMA (cells with green color, Fig. 3 & Supporting Information Fig. S3).

We next analyzed expression of collagen III (Col III), which is produced by myofibroblasts before synthesis of mechanically stronger collagen I. Expression of Col III was detected in wound bed (Supporting Information Fig. S4A, C, E) and granulation tissue (Supporting Information Fig. S4A, D, F), though the signal was weak. Expression of Col III was detected in the outside of wounded area (Supporting Information Fig. S4A & B). Transdifferentiation of ASC to endothelial cells was addressed using a platelet endothelial cell adhesion molecule (PECAM-1, CD31) - specific antibody. Expression of CD31 was prominently detected in the granulation tissue (Fig. 6G & Supporting Information Fig. S5). However, co-expression of CD31 in transplanted ASC was not detected (Supporting Information Fig. S5). Thus, transdifferentiation of transplanted ASC to endothelial cell was not found at POD7 in the rabbit wounds. Proliferation of transplanted ASC was detected with Ki-67 or PCNA specific antibodies (Fig. 4 & Supporting Information Fig. S6).

ASC enhance granulation tissue formation in wounds

To determine the optimal quantity of ASC to promote wound healing, we treated wounds with different amounts of ASC. Though we showed the conservation of surface markers of ASC *in vitro*, we used an early passage (P3) ASC in these experiments to avoid changes of characteristics of ASC over the long term *in vitro* culture. ASC were harvested, washed in PBS to remove cell culture medium, and resuspended in PBS. Three different amounts of ASC - 3×10^5, 1×10^5, and 3×10^4 - in 7 μl of PBS were delivered to each 7 mm wound of one ear. In the contralateral ear, 7 μl of PBS were delivered to each wound as a control. Wounds were harvested at POD7 and histological differences

such as epithelial gap and granulation tissue areas were digitally quantified as previously described (Supporting Information Fig. S7) [23, 24]. All three numbers of ASC increased granulation tissue area (data not shown). Wounds treated with highest ASC number - 3 x 10^5 - had a slightly higher epithelial gap. This means there was minor inhibition of keratinocyte migration, though this was statistically insignificant (data not shown).

To determine the dose of ASC which does not inhibit epithelialization but increases granulation tissue formation, wounds on one ear were treated with 1 x 10^5 ASC and wounds on the contralateral ear were treated with 3 x 10^4 ASC. Wounds with 1 x 10^5 ASC (n=11) had similar epithelial gaps (4.35 $\pm$ 0.42 mm, Supporting Information Fig. S8A) compared to wounds with 3 x 10^4 ASC (n=12, 4.09 $\pm$ 0.32 mm). However, wounds treated with 1 x 10^5 ASC showed greater granulation tissue area (Supporting Information Fig. S8B, 1.48 $\pm$ 0.21 vs. 0.95 $\pm$ 0.13 mm^2, p =0.09). Thus we determined that 1 x 10^5 ASC as an optimum number for wound healing study.

Next, we increased the number of wounds and animals to increase power of statistical analyses. With each rabbit serving as its own internal control, 1 x 10^5 of P3 ASC were delivered to wounds on one ear and the wounds on contralateral ear received saline alone as control as described above and wounds were analyzed at POD7. We compared between ears on the same animal for the histomorphological analysis to minimize the effects of rabbit-to-rabbit variation in wound healing. When compared to saline treated control wounds, ASC treated wounds showed increased granulation tissue area (0.50 $\pm$ 0.07 mm^2 vs. 1.13 $\pm$ 0.14 mm^2, Fig. 5A). ASC treatment did not affect epithelialization of the epidermis when compared to saline treated wounds (4,026 $\pm$ 306 µm vs. 3,913 $\pm$ 259 µm, respectively; p =0.8, Supporting Information Fig. S9). For

comparison, 1×10^5 of P3 BM-MSC (or DF) were delivered to wounds on one ear and saline control were delivered to wounds on the contralateral ear. We found that granulation tissue area was not significantly changed by BM-MSC (0.96 ± 0.32 mm^2 vs. 1.15 ± 0.13 mm^2, Fig. 5B) or DF (0.62 ± 0.10 mm^2 vs. 0.70 ± 0.10 mm^2, Fig. 5C) treatment when compared to saline treated wounds.

ASC treatment increased recruitment of macrophages

We further analyzed ASC treated wounds immunohistochemically and compared them with saline treated wounds. Expression of α-SMA was found in the granulation tissue of ASC treated wounds and saline treated control wounds (Fig. 6A, E). α-SMA signals in ASC treated wounds (Fig. 6E) are from endogenous activated fibroblast cells and transplanted ASC (Fig. 3 & Supporting Information Fig. S3). α-SMA signals in Fig. 6A are from endogenous activated fibroblast cells. The transplanted ASC are allogeneic because syngeneic rabbits are not available. We investigated whether transplanted allogeneic ASC evoke immune reactions *in vivo*, though immune modulatory property of ASC has been proposed [13, 15, 16]. Neither CD3 (T cell antigen) nor CD45 (common leukocyte antigen) positive signals were found by their specific antibodies in ASC treated wounds at POD7 (Fig. 6F & data not shown). Angiogenesis is one of critical factors in wound repair process. Blood vessel formation in granulation tissue, which is determined by endothelial marker (CD31) staining, was detected in ASC treated wounds and control wounds (Fig. 6C, G). Interestingly, a few CD31 positive cells were found in the wound beds of ASC treated wounds, though blood vessel structure was not found (Fig. 6H). In contrast, we could not detect CD31 positive cells in the wound beds of saline treated

wounds at POD7 (Fig. 6D). Since transdifferentiation of ASC to endothelial cells was not found at POD7 in our animal model (Supporting Information Fig. S5), we suggest that ASC increase endothelial cell recruitment in wounds.

Neutrophils migrate to wounded sites upon injury and initiate an initial inflammatory phase for wound repair. Then, macrophages move to the sites and secrete cytokines and growth factors which attract cells involved in wound repair [28, 29]. They participate in remodeling the extracellular matrix and forming granulation tissue to repair wounds. We did not detect a significant number of neutrophils at POD7 wounds in which ASC or saline controls were treated (Fig. 7A, B). We detected average of 16.4 macrophages in the granulation tissue near to the migrating epidermis with high power microscopic fields (HPF, Fig. 7C, E). The number of macrophages in the granulation tissue was markedly increased by ASC treatment at POD7 (Fig. 7D, E). Thus, our wound analyses (through Figs. 3 to 7) suggest that transplanted ASC exhibit the activated fibroblast phenotype and enhance wound repair by macrophage recruitment.

DISCUSSION

BM-MSC were first isolated among various MSC and have potential to contribute to wound repair in many tissues. However, the procedure for extracting BM-MSC is relatively invasive and could cause patient morbidity. Extended time is required to expand BM-MSC in culture to get a large enough number of cells for clinical uses. ASC have several advantages compared with BM-MSC because they are easy to isolate with relative abundance [6, 11, 21]. ASC and BM-MSC have similar surface markers,

cytokines and gene expression profiles [6, 13]. Thus, we selected ASC as a cell therapy reagent for wound repair in this report and compared their properties to BM-MSC. The mesodermal lineage differentiation experiment suggests that ASC are more likely to differentiate into adipocytes, while BM-MSC are prone to differentiate into chondrocytes (Fig. 2). ASC engrafts enhanced granulation tissue area in rabbit ear wounds, while BM-MSC engrafts did not increase granulation tissue area (Fig. 5). Our results further support the finding suggesting ASC and BM-MSC are not identical, though they have similar surface markers [30-32]. DF are poorly characterized diverse cells which locate in dermis. Upon injury DF are activated and become myofibroblasts, which express α-SMA and cytokines while depositing extracellular matrix [33]. It has been shown that human ASC and DF display similar surface markers and multipotency to differentiate into osteocytes, adipocytes, and chondrocytes [34-36]. They have similar chemokine expression profiles. However despite the morphological similarity, they are not identical [37, 38]. Our analysis showed that DF have less potency to be differentiated compared to ASC and BM-MSC (Fig. 2). While the use of DF in wound repair has been reported [24, 39], the DF engraft did not enhance granulation tissue area in rabbit ear wounds (Fig. 5)

Though MSC themselves are multipotent, the interactions between MSC and their environment are important for maintaining the proper function of MSC, i.e., differentiation into various cell types and production of signaling molecules. It has been shown that biocompatible and biodegradable matrices can support the growth of MSC. Extracellular matrices, synthetic or naturally derived, have served effectively as scaffolds for cell delivery and formation of new tissue [1, 40]. Enhanced wound healing by stem cells seeded on matrices has been reported [20, 41]. We performed experiments to find

optimum delivery vehicles for ASC in rabbit ear wounds. We selected fibrin as delivery vehicle. Fibrin is a natural biopolymer of blood proteins fibrinogen and thrombin and has been used as a vehicle to deliver fibroblasts, keratinocytes, and MSC [25, 42, 43]. The delivery vehicle should have neither beneficial nor adverse effects in promoting wound healing in order to see the true effect of ASC in the healing process. For that purpose, we delivered fibrin alone or saline alone to rabbit wounds as previously described [24, 25]. Fibrin sealant treated wounds showed similar results in wound healing parameter analysis when compared with saline treated wounds (data not shown). Next, we delivered 1×10^5 ASC to wounds in fibrin or saline and found that there were not significant differences in epithelialization. However, more granulation areas were found in wounds where ASC were delivered in fibrin when compared to wounds treated with ASC in saline (data not shown). We expect that several potential problems might be found in fibrin as a ASC delivery vehicle in rabbit wounds: 1) fibrinogen and thrombin are human origin, which may evoke inflammation, 2) the purity and quality of fibrinogen and thrombin will not be same among vendors, 3) optimum condition of fibrinogen and thrombin for ASC can be different, even though we used conditions based on our previous publication in which fibroblasts were used [24, 25]. Thus, we used saline as a vehicle of ASC in the study.

There are several pitfalls to be addressed, even though ASC are a promising candidate for cell therapy. First, it is expected that engrafted ASC participate in wound repair by either paracrine signaling or direct differentiation to specific cell types such as endothelial cells or keratinocytes. There are reports which showed transdifferentiation of ASC *in vivo* [20, 44]. However, it is speculated that the major role of engrafted ASC is secreting cytokine and growth factors, which enhance wound repair (see the following

paragraph). Multipotency of ASC has been tested *in vitro* where signals are provided to differentiate ASC to specific cell types; however, this is unlikely to happen *in vivo*. Therefore, further investigation to find the optimum microenvironment for ASC differentiation is essential in the complex and multicellular process of wound repair. Second, allogeneic and xenogeneic therapeutics have been considered because they have reduced expression of histocompatibility antigens and secrete immunoregulatory molecules [10, 15, 16]. However, investigation of immune reaction by comparing autologous ASC in quantitative analysis is needed. Third, a limiting factor of ASC is that they differ in proliferation and differentiation capacity depending on age, gender, and the location in the body from which the cells are derived [45-47]. Understanding the underlining mechanisms, such as epigenetic control, is needed for the clinical use of non-autologous ASC.

Though there are disputes on transdifferentiation of ASC *in vivo*, costaining of engrafted ASC with other cell types has been reported *in vivo*. ASC are differentiated to endothelial and epidermal cells in the murine model 2-4 weeks after delivery [20]. However, costaining of ASC with endothelial marker was not found in the rabbit wounds 7 days after delivery (Supporting Information Fig. S5). Therefore, we suspect that 7 days are not enough for rabbit ASC to be transdifferentiated to other cells or that the microenvironment in rabbit wounds is different from that in murine wounds. There are reports which suggest that engrafted ASC enhance angiogenesis by releasing angiogenic factors [17, 48, 49]. In line with this, we found increased CD31 positive cells in wound bed in ASC treated wounds (Fig. 6H), though direct differentiation of ASC to endothelial cells was not detected. It has been suggested that MSC contribute to tissue repair via

secretion of soluble factors rather than transdifferentiation [7, 50]. We anticipate that the paracrine effect of ASC in wound healing is crucial for the healing of wounds in which large volume of tissues is lost.

Macrophages play key roles during the wound repair process which includes inflammation, granulation formation, and remodeling in wounds [28]. It has been shown that macrophages promote wound repair after skin injury [51-54]. Myofibroblasts are activated fibroblasts and express α-SMA. They play a critical role in wound repair by depositing extracellular matrices such as fibronectin and collagen, and by secreting proteinases which remodel the matrix [55]. Thus, both myofibroblasts and macrophages are critical players in wound repair. Engrafted ASC showed the myofibroblast phenotype in rabbit ear wound (Fig. 3). In addition, the number of infiltrated macrophages was increased in ASC treated wounds (Fig. 7). These data suggest that transplanted ASC enhance granulation tissue formation via their activated fibroblast phenotype and increased recruitment of macrophages in wounds.

CONCLUSIONS

ASC have advantages as cell therapy agents as compared with other MSC, such as BM-MSC. This is because they are easy to isolate with relative abundance. We confirmed that MSC surface markers (CD29, CD44, CD 90, and CD105) are expressed in rabbit ASC and are maintained in *in vitro* culture. Rabbit ASC have the ability to differentiate into mesodermal cells such as adipocytes, chondrocytes, and osteocytes. Topically delivered ASC proliferated in the wounds exhibit the activated fibroblast phenotype. Engrafted

ASC increased macrophage recruitment and enhanced granulation tissue formation in wounds. Our data support ASC as a possible cell therapy candidate for the repair of wounds.

DISCLOSURE OF POTENTIAL CONFLICTS OF INTEREST

The authors indicate no potential conflicts of interest.

REFERENCES

1. Gurtner GC, Werner S, Barrandon Y, et al. Wound repair and regeneration. Nature. 2008;453:314-321.

2.   Werner S, Grose R. Regulation of wound healing by growth factors and cytokines. Physiol Rev. 2003;83:835-870.

3.   Singer AJ, Clark RA. Cutaneous wound healing. N Engl J Med. 1999;341:738-746.

4.   Gurtner GC, Callaghan MJ, Longaker MT. Progress and potential for regenerative medicine. Annu Rev Med. 2007;58:299-312.

5.   Stappenbeck TS, Miyoshi H. The role of stromal stem cells in tissue regeneration and wound repair. Science. 2009;324:1666-1669.

6.   Meliga E, Strem BM, Duckers HJ, et al. Adipose-derived cells. Cell Transplant. 2007;16:963-970.

7.   Phinney DG, Prockop DJ. Concise review: mesenchymal stem/multipotent stromal cells: the state of transdifferentiation and modes of tissue repair--current views. Stem Cells. 2007;25:2896-2902.

8.   Pittenger MF, Mackay AM, Beck SC, et al. Multilineage potential of adult human mesenchymal stem cells. Science. 1999;284:143-147.

9.   Bunnell BA, Estes BT, Guilak F, et al. Differentiation of adipose stem cells. Methods Mol Biol. 2008;456:155-171.

10.   Caplan AI. Why are MSCs therapeutic? New data: new insight. J Pathol. 2009;217:318-324.

11.   Brown SA, Levi B, Lequeux C, et al. Basic science review on adipose tissue for clinicians. Plast Reconstr Surg. 2010;126:1936-1946.

12.   Lindroos B, Suuronen R, Miettinen S. The potential of adipose stem cells in regenerative medicine. Stem Cell Rev. 2011;7:269-291.

13. Gimble JM, Katz AJ, Bunnell BA. Adipose-derived stem cells for regenerative medicine. Circulation Research. 2007;100:1249-1260.

14. Rehman J, Traktuev D, Li J, et al. Secretion of angiogenic and antiapoptotic factors by human adipose stromal cells. Circulation. 2004;109:1292-1298.

15. McIntosh K, Zvonic S, Garrett S, et al. The immunogenicity of human adipose-derived cells: temporal changes in vitro. Stem Cells. 2006;24:1246-1253.

16. Puissant B, Barreau C, Bourin P, et al. Immunomodulatory effect of human adipose tissue-derived adult stem cells: comparison with bone marrow mesenchymal stem cells. Br J Haematol. 2005;129:118-129.

17. Le Blanc K, Mougiakakos D. Multipotent mesenchymal stromal cells and the innate immune system. Nat Rev Immunol. 2012;12:383-396.

18. Zuk PA. The adipose-derived stem cell: looking back and looking ahead. Mol Biol Cell. 2010;21:1783-1787.

19. Mizuno H, Tobita M, Uysal AC. Concise review: Adipose-derived stem cells as a novel tool for future regenerative medicine. Stem Cells. 2012;30:804-810.

20. Altman AM, Yan Y, Matthias N, et al. IFATS collection: Human adipose-derived stem cells seeded on a silk fibroin-chitosan scaffold enhance wound repair in a murine soft tissue injury model. Stem Cells. 2009;27:250-258.

21. Locke M, Feisst V, Dunbar PR. Concise review: human adipose-derived stem cells: separating promise from clinical need. Stem Cells. 2011;29:404-411.

22. Nambu M, Ishihara M, Nakamura S, et al. Enhanced healing of mitomycin C-treated wounds in rats using inbred adipose tissue-derived stromal cells within an atelocollagen matrix. Wound Repair Regen. 2007;15:505-510.

23. Sisco M, Mustoe TA. Animal models of ischemic wound healing. Toward an approximation of human chronic cutaneous ulcers in rabbit and rat. Methods Mol Med. 2003;78:55-65.

24. Steinberg JP, Hong SJ, Geringer MR, et al. Equivalent effects of topically-delivered adipose-derived stem cells and dermal fibroblasts in the ischemic rabbit ear model for chronic wounds. Aesthet Surg J. 2012;32:504-519.

25. Mogford J, Tawill B, Jia X, et al. Fibrin sealant combined with fibroblast and platelet-derived growth factor enhance wound haealing in excisional wounds. Wound Rep Reg. 2009;17:405-410.

26. Li B, Wang JH. Fibroblasts and myofibroblasts in wound healing: force generation and measurement. J Tissue Viability. 2011;20:108-120.

27. Sarrazy V, Billet F, Micallef L, et al. Mechanisms of pathological scarring: role of myofibroblasts and current developments. Wound Repair Regen. 2011;19 Suppl 1:s10-15.

28. Mahdavian Delavary B, van der Veer WM, van Egmond M, et al. Macrophages in skin injury and repair. Immunobiology. 2011;216:753-762.

29. Brancato SK, Albina JE. Wound macrophages as key regulators of repair: origin, phenotype, and function. Am J Pathol. 2011;178:19-25.

30. Nakao N, Nakayama T, Yahata T, et al. Adipose tissue-derived mesenchymal stem cells facilitate hematopoiesis in vitro and in vivo: advantages over bone marrow-derived mesenchymal stem cells. Am J Pathol. 2010;177:547-554.

31. Ikegame Y, Yamashita K, Hayashi S, et al. Comparison of mesenchymal stem cells from adipose tissue and bone marrow for ischemic stroke therapy. Cytotherapy. 2011;13:675-685.

32. Strioga M, Viswanathan S, Darinskas A, et al. Same or Not the Same? Comparison of Adipose Tissue-Derived Versus Bone Marrow-Derived Mesenchymal Stem and Stromal Cells. Stem Cells Dev. 2012.

33. Werner S, Krieg T, Smola H. Keratinocyte-fibroblast interactions in wound healing. J Invest Dermatol. 2007;127:998-1008.

34. Kroeze KL, Jurgens WJ, Doulabi BZ, et al. Chemokine-mediated migration of skin-derived stem cells: predominant role for CCL5/RANTES. J Invest Dermatol. 2009;129:1569-1581.

35. Hasebe Y, Hasegawa S, Hashimoto N, et al. Analysis of cell characterization using cell surface markers in the dermis. J Dermatol Sci. 2012;62:98-106.

36. Haniffa MA, Wang XN, Holtick U, et al. Adult human fibroblasts are potent immunoregulatory cells and functionally equivalent to mesenchymal stem cells. J Immunol. 2007;179:1595-1604.

37. Hsiao ST, Asgari A, Lokmic Z, et al. Comparative Analysis of Paracrine Factor Expression in Human Adult Mesenchymal Stem Cells Derived from Bone Marrow, Adipose, and Dermal Tissue. Stem Cells Dev. 2012.

38. van der Bogt KE, Schrepfer S, Yu J, et al. Comparison of transplantation of adipose tissue- and bone marrow-derived mesenchymal stem cells in the infarcted heart. Transplantation. 2009;87:642-652.

39.   Lee SH, Lee JH, Cho KH. Effects of Human Adipose-derived Stem Cells on Cutaneous Wound Healing in Nude Mice. Ann Dermatol. 2011;23:150-155.

40.   Discher DE, Mooney DJ, Zandstra PW. Growth factors, matrices, and forces combine and control stem cells. Science. 2009;324:1673-1677.

41.   Altman AM, Matthias N, Yan Y, et al. Dermal matrix as a carrier for in vivo delivery of human adipose-derived stem cells. Biomaterials. 2008;29:1431-1442.

42.   Currie LJ, Sharpe JR, Martin R. The use of fibrin glue in skin grafts and tissue-engineered skin replacements: a review. Plast Reconstr Surg. 2001;108:1713-1726.

43.   Gwak SJ, Kim SS, Sung K, et al. Synergistic effect of keratinocyte transplantation and epidermal growth factor delivery on epidermal regeneration. Cell Transplant. 2005;14:809-817.

44.   Ebrahimian TG, Pouzoulet F, Squiban C, et al. Cell therapy based on adipose tissue-derived stromal cells promotes physiological and pathological wound healing. Arterioscler Thromb Vasc Biol. 2009;29:503-510.

45.   Giorgino F, Laviola L, Eriksson JW. Regional differences of insulin action in adipose tissue: insights from in vivo and in vitro studies. Acta Physiol Scand. 2005;183:13-30.

46.   Chen L, Peng EJ, Zeng XY, et al. Comparison of the proliferation, viability, and differentiation capacity of adipose-derived stem cells from different anatomic sites in rabbits. Cells Tissues Organs. 2012;196:13-22.

47. Roldan M, Macias-Gonzalez M, Garcia R, et al. Obesity short-circuits stemness gene network in human adipose multipotent stem cells. Faseb J. 2011;25:4111-4126.

48. Nakagami H, Maeda K, Morishita R, et al. Novel autologous cell therapy in ischemic limb disease through growth factor secretion by cultured adipose tissue-derived stromal cells. Arterioscler Thromb Vasc Biol. 2005;25:2542-2547.

49. Cai L, Johnstone BH, Cook TG, et al. Suppression of hepatocyte growth factor production impairs the ability of adipose-derived stem cells to promote ischemic tissue revascularization. Stem Cells. 2007;25:3234-3243.

50. Hocking AM, Gibran NS. Mesenchymal stem cells: paracrine signaling and differentiation during cutaneous wound repair. Exp Cell Res. 2010;316:2213-2219.

51. Mirza R, DiPietro LA, Koh TJ. Selective and specific macrophage ablation is detrimental to wound healing in mice. Am J Pathol. 2009;175:2454-2462.

52. Ishida Y, Gao JL, Murphy PM. Chemokine receptor CX3CR1 mediates skin wound healing by promoting macrophage and fibroblast accumulation and function. J Immunol. 2008;180:569-579.

53. Danon D, Kowatch MA, Roth GS. Promotion of wound repair in old mice by local injection of macrophages. Proc Natl Acad Sci U S A. 1989;86:2018-2020.

54. Lucas T, Waisman A, Ranjan R, et al. Differential roles of macrophages in diverse phases of skin repair. J Immunol. 2010;184:3964-3977.

55. Schafer M, Werner S. Cancer as an overhealing wound: an old hypothesis revisited. Nat Rev Mol Cell Biol. 2008;9:628-638.

Figure 1. Morphology and surface markers of rabbit MSC. **(A-C):** Bright field images of rabbit ASC (A), BM-MSC (B), and DF (C). Cells were grown in culture dishes with growth medium and photos were taken. Scale bar; 100 μm. **(D):** Western blot analysis. Whole cell extract of rabbit ASC from passage 1 (P1) to P9 was prepared and loaded 20 μg per well. The expression of CD29, CD44, CD90, and CD105 were detected with their specific antibodies as indicated. β-actin was detected as a loading control.

Figure 2. Rabbit MSC differentiate to mesodermal lineages *in vitro*. Passage 2 ASC (A, D, G), BM-MSC (B, E, H), and DF (C, F, I) were used for differentiation. **(A-C):** Adipogenic differentiation. Cells were cultured in adipogenesis differentiation medium for 8 days. Oil Red O staining was performed to detect lipid accumulation. Nuclei were stained with Hematoxylin. **(D-F):** Chondrogenic differentiation. Cells were cultured in chondrogenesis differentiation medium for 21 days. Alician blue staining was performed. **(G-I):** Osteogenic differentiation. Cells were cultured in osteogenesis differentiation medium for 35 days. Alizarin Red S staining was performed to detect calcium accumulation. Abbreviation: MSC, mesenchymal stem cell; ASC, adipose derived stem cell; DF, dermal fibroblast; BM-MSC, bone marrow derived mesenchymal stem cell. Scale bar; (A-F) 50 μm, (G-I) 100 μm.

Figure 3. Transplanted ASC express α-SMA in wounds. GFP-expressing ASC were analyzed 7 days after transplantation in wounds. Chicken anti-GFP and mouse anti-α-SMA antibodies were used to detect GFP and α-SMA. Nuclei were stained with DAPI. **(A):** Low magnification of wounds. The areas analyzed in Figure 6 were indicated by 'a' and 'b'. **(B-D):** Higher magnifications of the indicated regions in A (white squares; labeled as i, ii, iii). **(E-G):** Higher magnifications of the indicated regions in B-D (white squares; labeled as iv, v, vi). Merged images of α-SMA (red) and GFP (green) indicate that α-SMA is expressed in ASC. Scale bars: 500 μm (A), 50 μm (B-G).

Figure 4. Transplanted ASC proliferate in wounds. GFP-expressing ASC were analyzed 7 days after transplantation in wounds. Chicken anti-GFP (A) and mouse anti-Ki67 (C) antibodies were used. Nuclei were stained with DAPI (B). Merged image was shown in D. Scale bars: 50 μm.

Figure 5. Histological quantification of MSC treated wounds. **(A-C):** A total of 1×10^5 ASC (A), BM-MSC (B), and DF (C) in PBS were delivered to 7 mm wounds on one ear. In the contralateral ear, PBS alone was delivered as a control. Wounds were harvested at POD7 and granulation tissue area was measured. Number of wounds analyzed; (A, n=35 for saline & n=36 for ASC; B, n=17 for saline & n=20 for BM-MSC, C, n=17 for saline & n=24 for DF). Data shown as mean $\pm$ SEM. ***p<0.001, ns = not significant.

Figure 6. Analysis of protein expression in ASC treated wounds. Saline control (A, B, C, D) and ASC (E, F, G, H) were delivered to wounds and harvested as described in Figure

5. α-SMA (A, E) and CD3 (B, F) were visualized by DAB after staining with their specific antibodies. CD31 (C, D, G, H) was stained with its specific antibody and visualized using fluorescence conjugated secondary antibody. **(A, B, C, E, F, G):** images were taken from the area labeled as 'a' in Figure 3. **(D, H):** Immunostaining for CD31 in the area labeled as 'b' in Figure 3. The junction area between cartilage and wound beds was demarcated by white dot lines. CD31 positive signals were indicated by arrows in H. Scale bars: 50 μm.

Figure 7. Higher infiltration of macrophages was found in ASC treated wounds. Saline control (A, C) and ASC (B, D) were delivered to wounds and harvested as described in Figure 5. Neutrophils **(A, B)** and macrophages **(C, D)** were visualized by DAB after staining with their specific antibodies. Scale bars: 100 μm. **(E):** Number of macrophages per high-power microscopic fields (HPF) at 400 X magnification. Macrophages were counted and averaged from four HPF. Data are from four independent wounds and presented as mean $\pm$ SEM. ***p<0.001.

Supplemental Figure S1. Western blot analysis for surface markers of rabbit BM-MSC. Whole cell extract of rabbit BM-MSC from P1 to P9 was prepared and loaded 20 μg per well. The expression of CD29, CD44, CD90, and CD105 were detected with their specific antibodies as indicated. β-actin was detected as a loading control.

Supplemental Figure S2. mRNA level of lineage specific genes was increased by differentiation in MSC. DF, ASC, and BM-MSC were grown in adipogenic (A), osteogenic (B), or chondrogenic (C) medium for 8, 28, or 21 days. Total RNAs were isolated and RT-qPCR was performed. Expression of adiponectin (A), osteopontin (B), and Col10a1 (C) was analyzed. Each gene expression was normalized according to the expression level of Gapdh. The level of gene expression in cells cultured in differentiation medium was compared to cells cultured in non-differentiated medium, which was set at 1.

Supplemental Figure S3. Analysis of α-SMA expressing cells in wounds. Chicken anti-GFP and mouse anti-α-SMA antibodies were used to detect GFP and α-SMA. Nuclei were stained with DAPI. GFP (A, D, G), α-SMA (B, E, H), and merged (C, F, I) images in Figure 3E, 3F, 3G were shown. Endogenous cells and transplanted ASC which express α-SMA showed red and yellow color, respectively, in the merged images (C, F, I). Transplanted ASC which do not express α-SMA showed green color in the merged images. Scale bars: 50 μm.

Supplemental Figure S4. Expression of collagen III (Col III) in wounds. GFP-expressing ASC were analyzed 7 days after transplantation in wounds. Chicken anti-GFP and mouse anti-Col III antibodies were used to detect GFP (green) and Col III (red). Nuclei were stained with DAPI. **(A):** Low magnification of wounds. **(B-D):** Higher magnifications of the indicated regions in A (white squares; labeled as i, ii, iii). **(E-F):** Higher magnifications of the indicated regions in C and D (white squares; labeled as iv

and v). Merged images of Col III and GFP were shown. Scale bars: 500 µm (A), 100 µm (B, C, D), 50 µm (E, F).

Supplemental Figure S5. Analysis of expression of CD31 (PECAM-1) in transplanted ASC. GFP-expressing ASC were analyzed 7 days after transplantation in wounds. Chicken anti-GFP (A, D) and mouse anti-CD31 (B, E) antibodies were used to detect GFP and CD31. Nuclei were stained with DAPI. Co-expression of CD31 and GFP was not detected in the merged images (C, F). Two examples, section 1 and section 2, were shown. Scale bar; 50 µm.

Supplemental Figure S6. Transplanted ASC proliferate in wounds. GFP-expressing ASC were analyzed 7 days after transplantation in wounds. Chicken anti-GFP (A) and mouse anti-PCNA (C) antibodies were used. Nuclei were stained with DAPI (B). Merged image was shown in D. Scale bars: 50 µm.

Supplemental Figure S7. Schematic drawing of rabbit wounds and histological analysis. EG, epithelial gap; GA, granulation area.

Supplemental Figure S8. Histological quantification of ASC treated wounds. 1×10^5 ASC were delivered to 7 mm wounds on one ear and 3×10^4 ASC were delivered to wounds on the contralateral ear of rabbits. Wounds were harvested at POD7 and epithelial gap (A) and granulation tissue area (B) were measured (n=11 for 1×10^5 ASC & n=12 for 3×10^4 ASC). Data shown as mean $\pm$ SEM. ns = not significant.

Supplemental Figure S9. Measurement of epithelial gap of ASC treated wounds. A total of 1 x 10^5 ASC were delivered to 7 mm wounds on one ear. In the contralateral ear, PBS alone was delivered as a control. Wounds were harvested at POD7 and epithelial gap was measured. Data shown as mean ± SEM. n=35 for saline & n=36 for ASC. ns = not significant.

ASC	BM-MSC	DF
A	B	C

D

	P1	P2	P3	P4	P5	P6	P7	P8	P9
CD29									
CD44									
CD90									
CD105									
β-actin									

Figure 1

	ASC	BM-MSC	DF
adipogenesis	A	B	C
chodrogenesis	D	E	F
osteogenesis	G	H	I
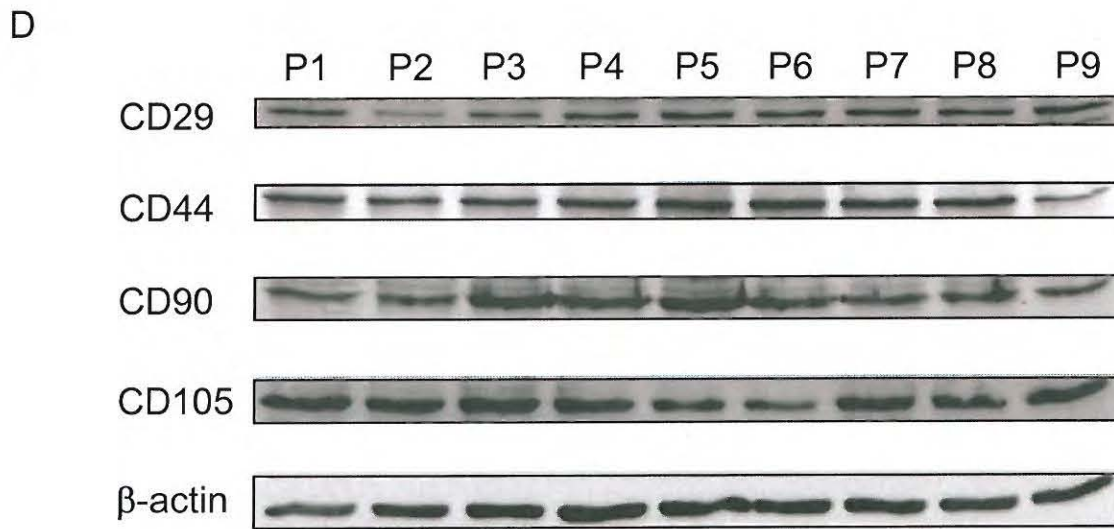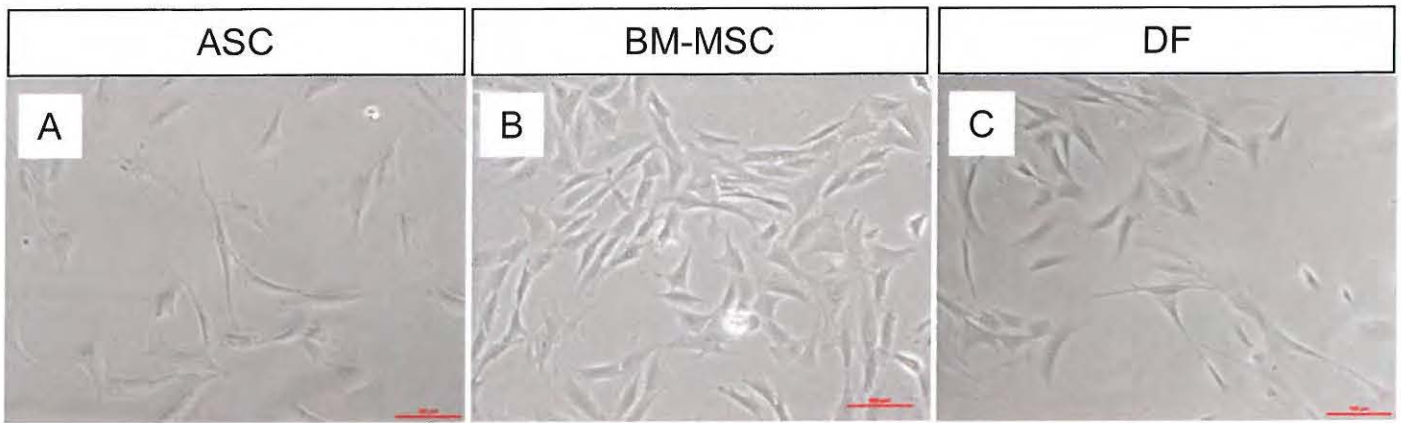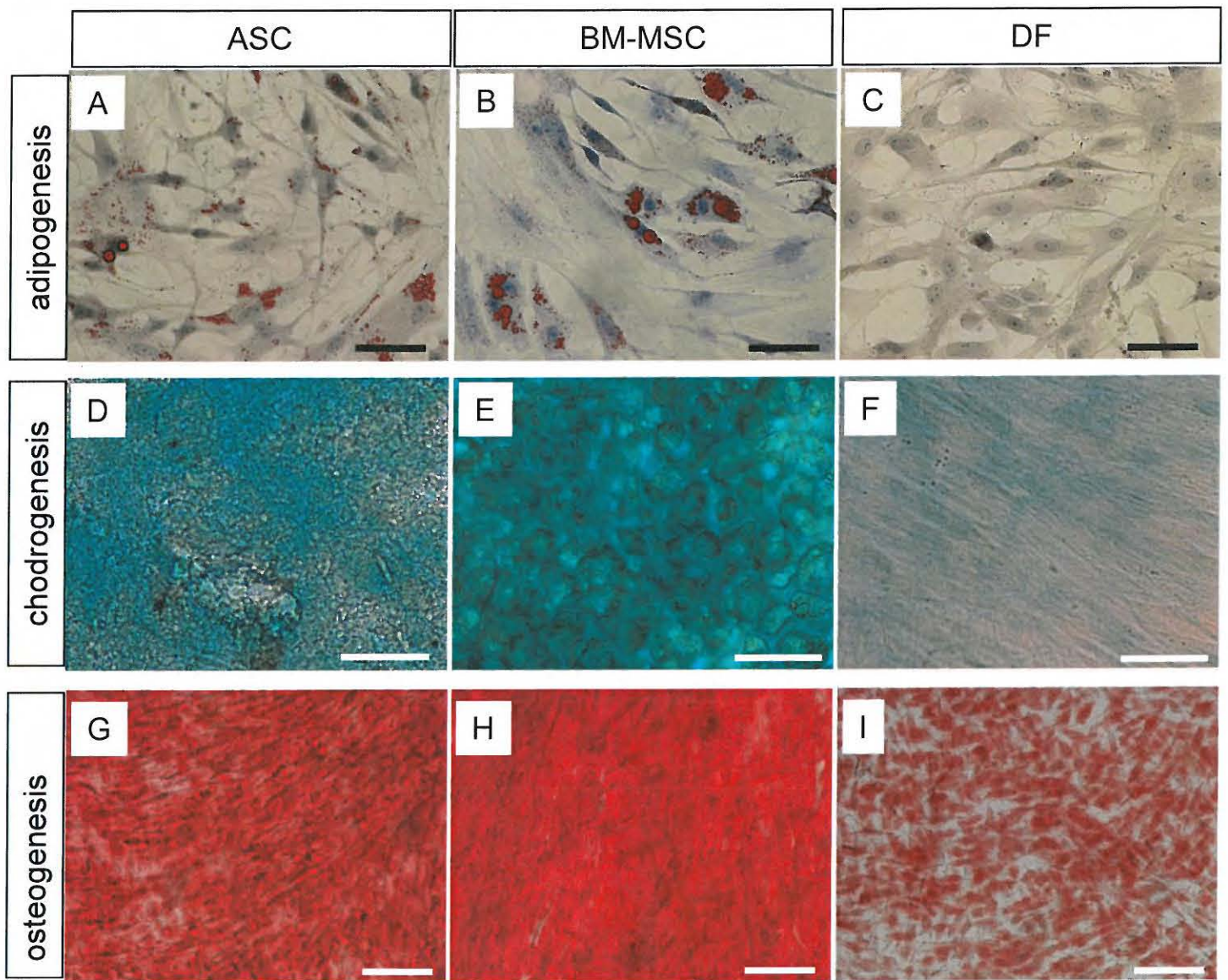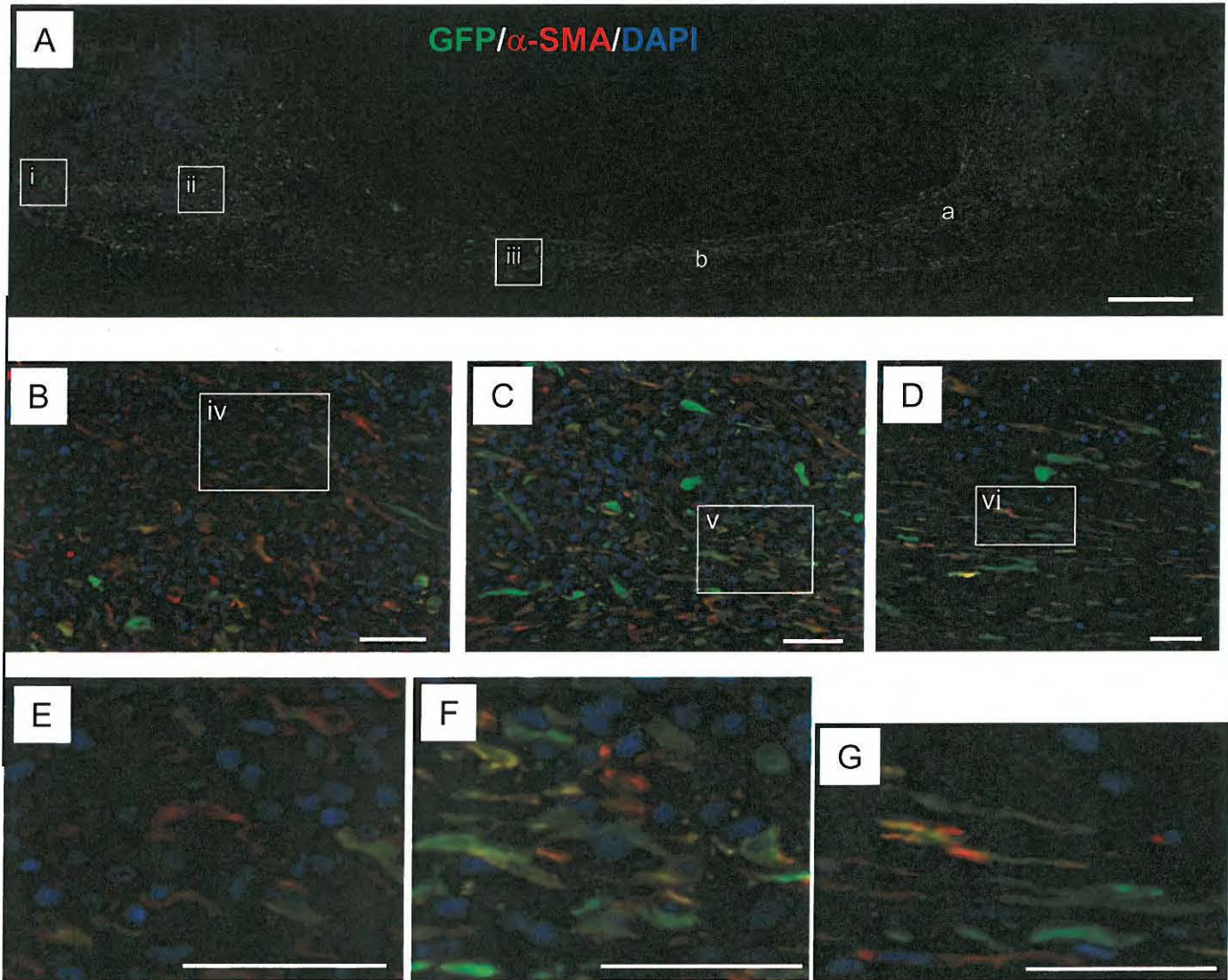
Figure 2

Figure 3

Figure 4

Figure 5

saline	ASC
A	E
B	F
C	G
D	H

α-SMA

CD3

CD31

CD31

cartilage

cartilage

Figure 6

saline | ASC

neutrophil

A | B

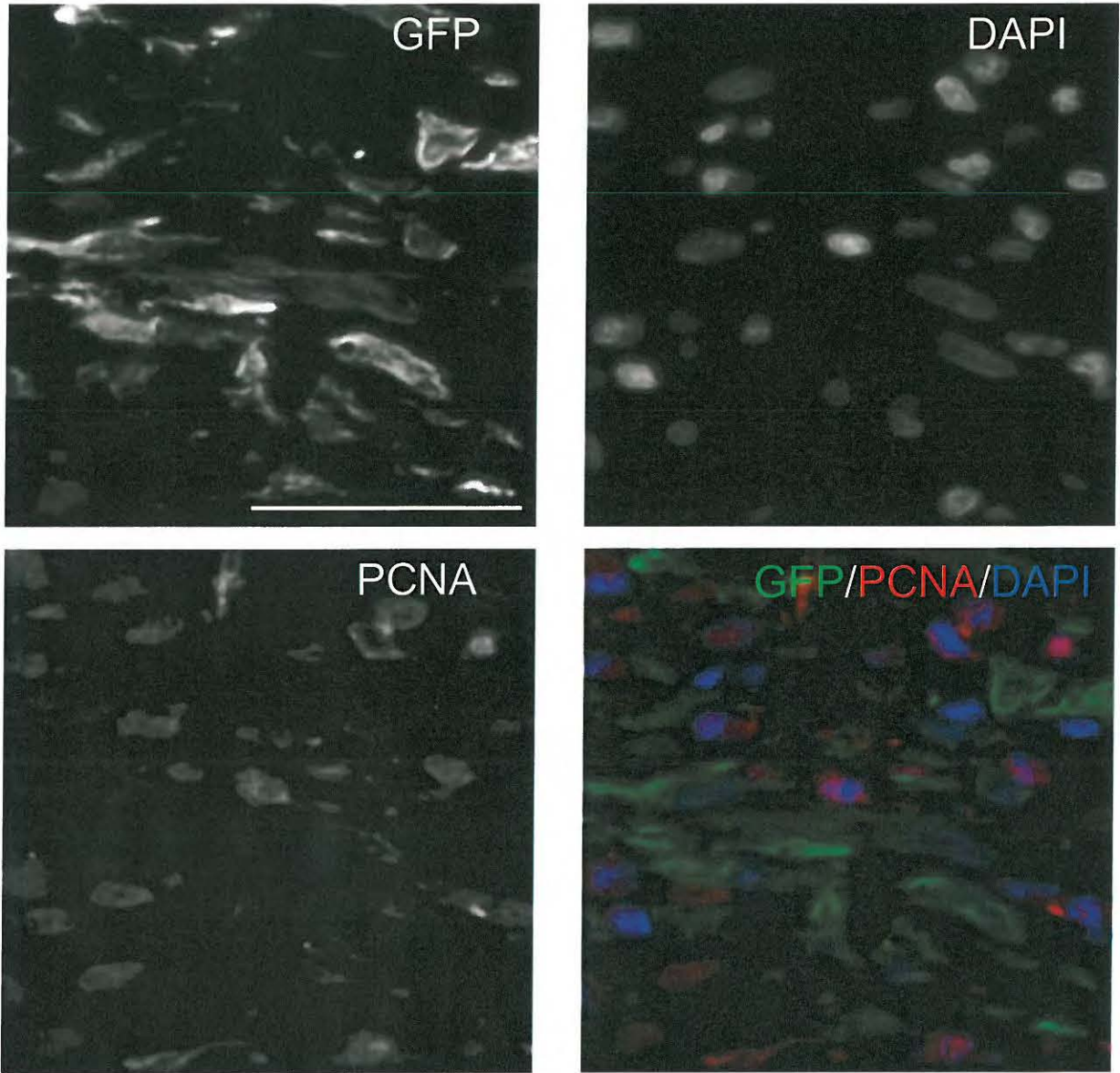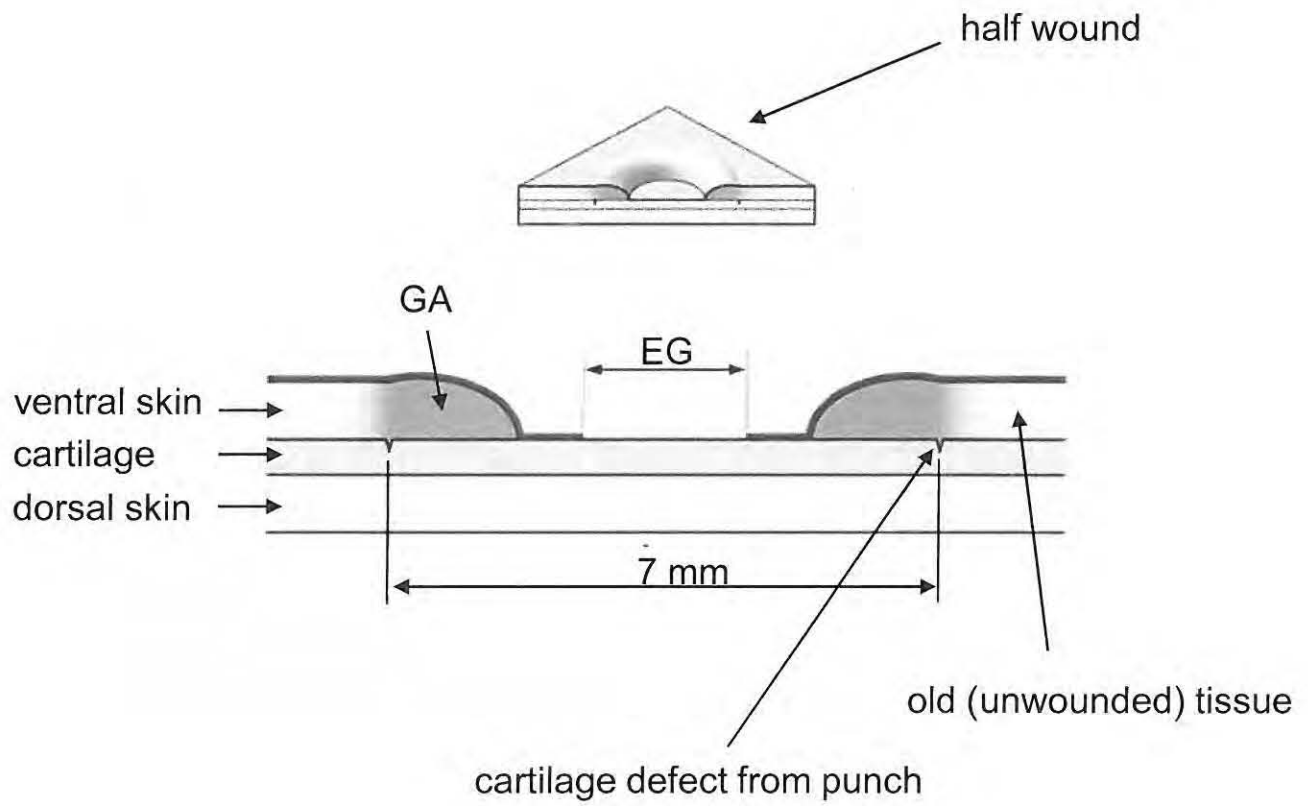macrophage
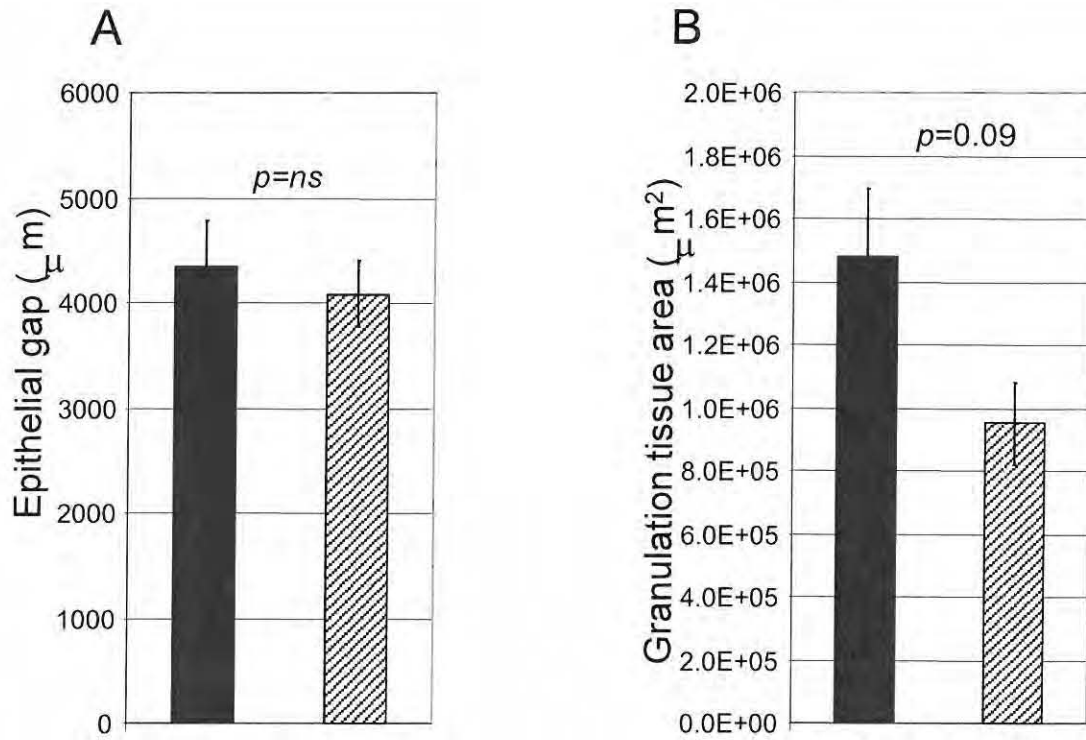
C | D

E
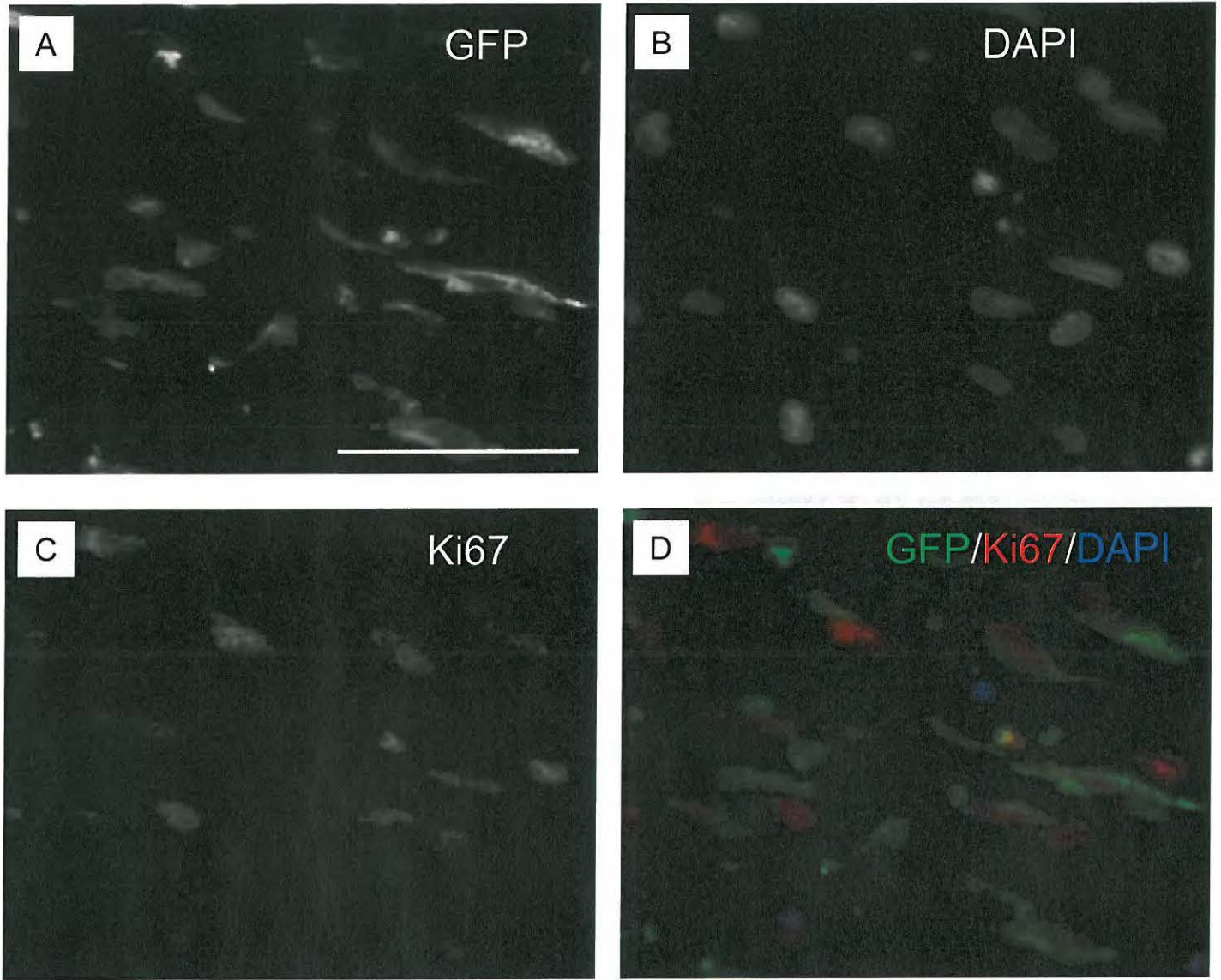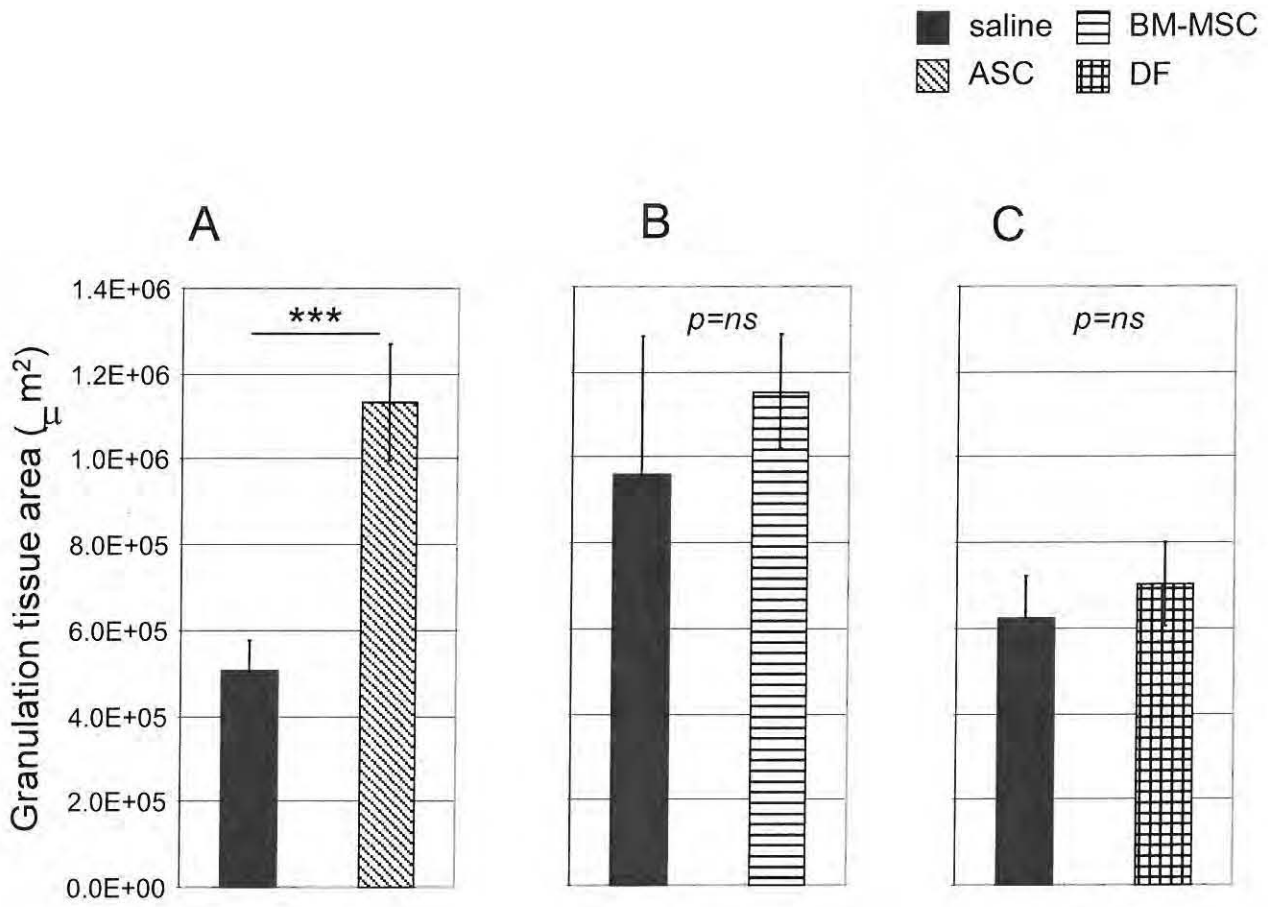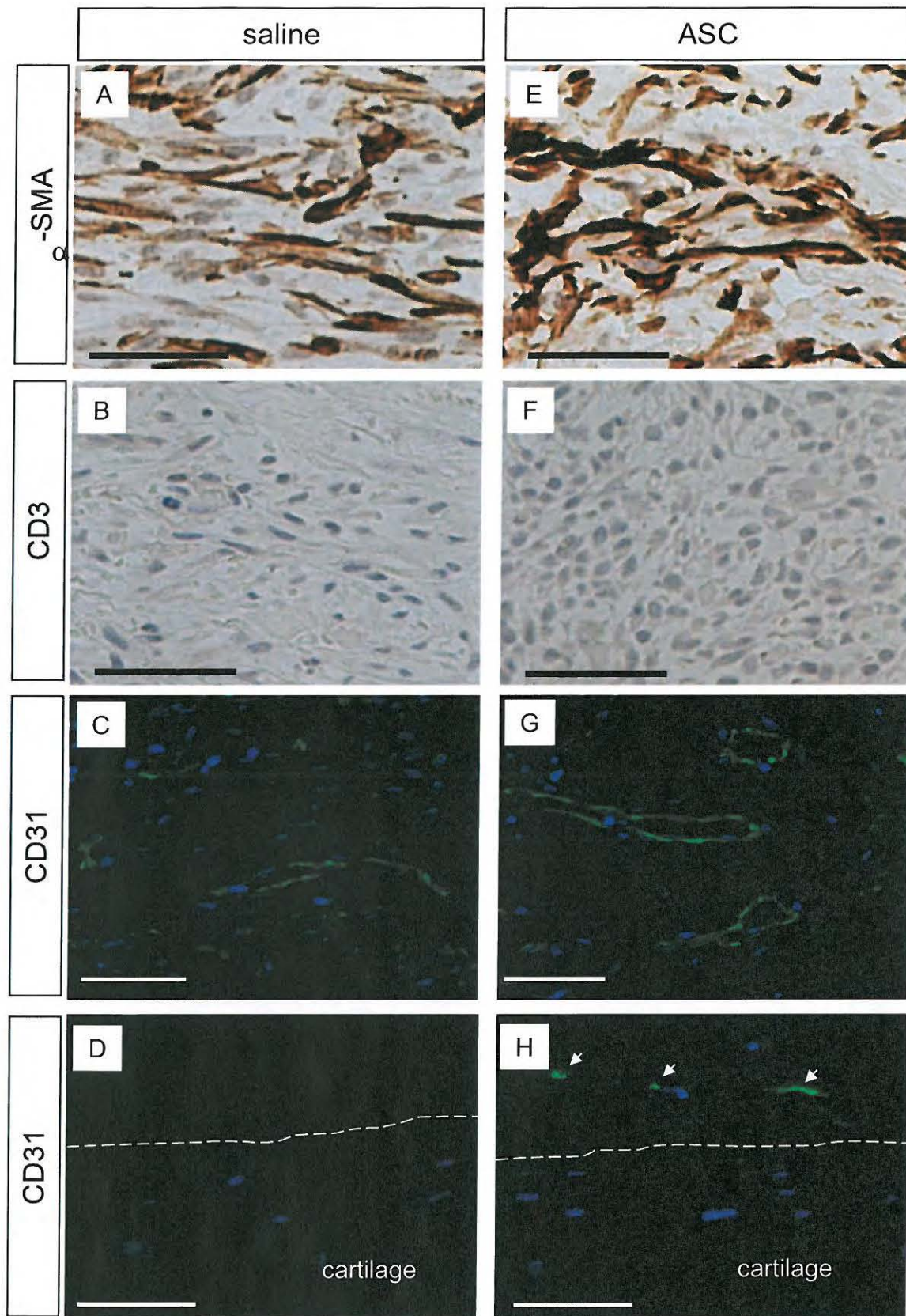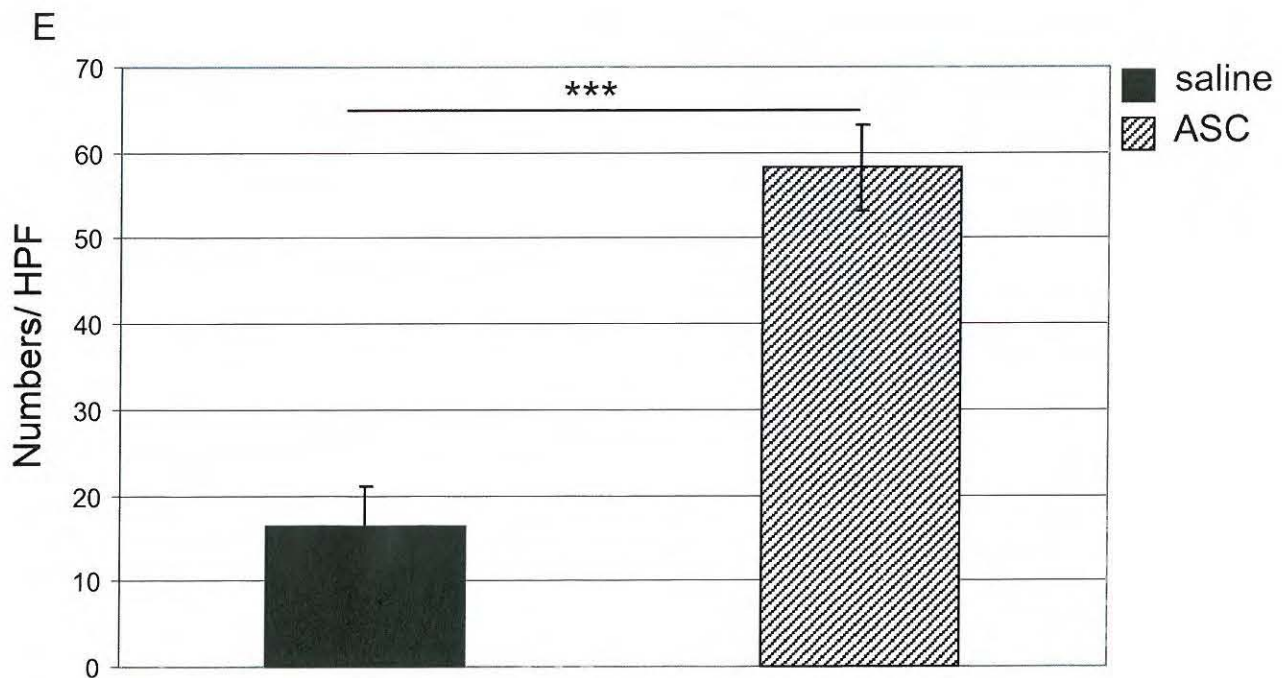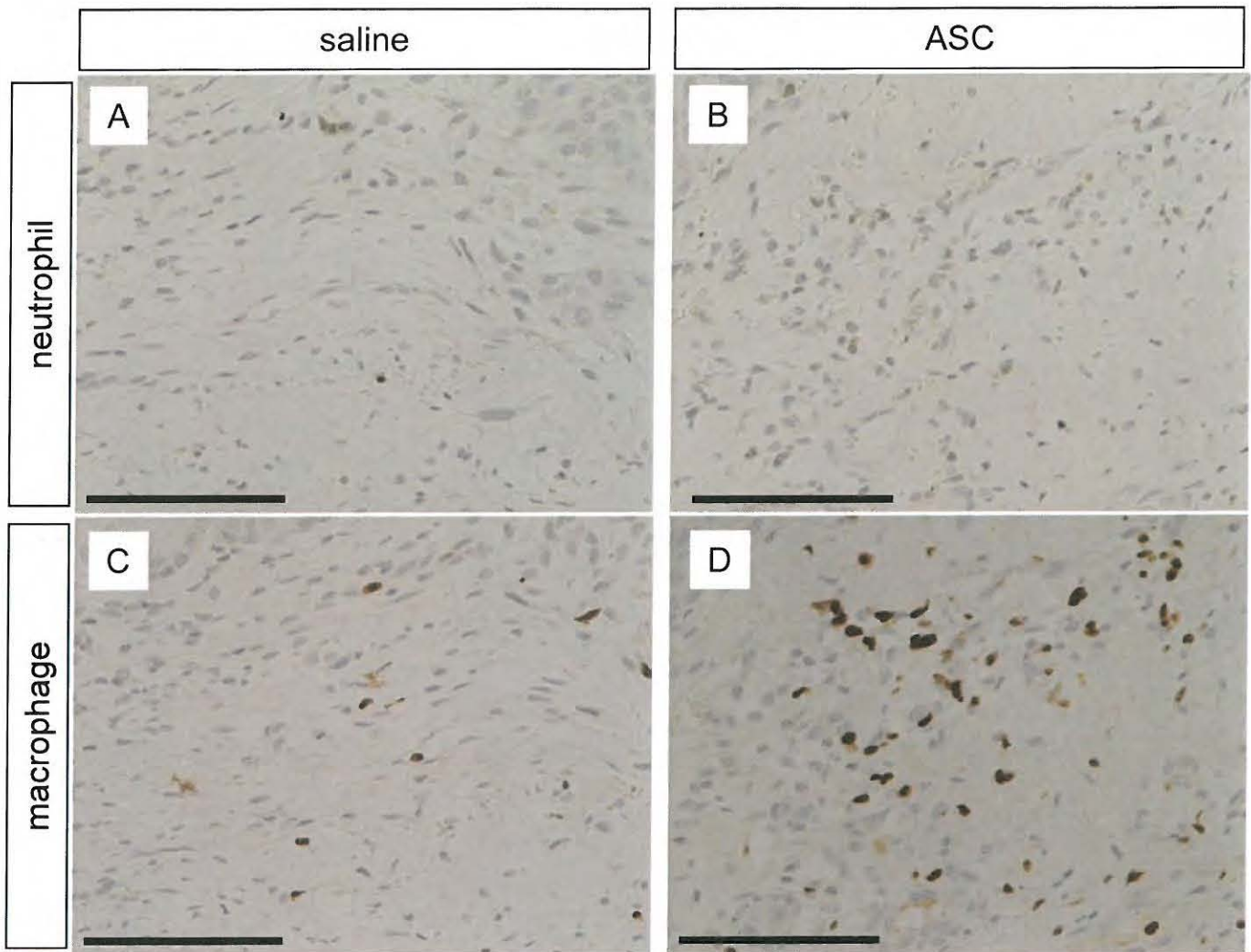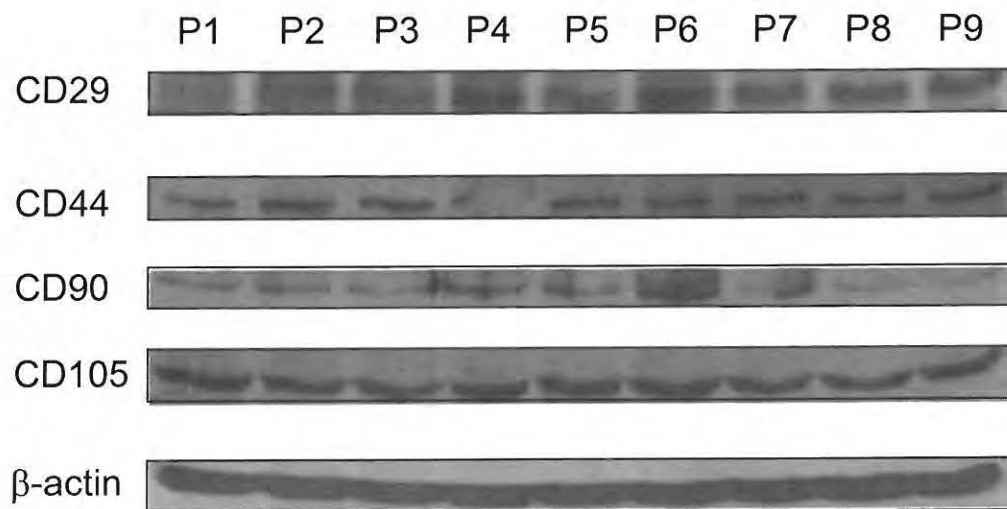
Figure 7

Supplemental Figure S1

Supplemental Figure S2

area i (Fig. 3E)	area ii (Fig. 3F)	area iii (Fig. 3G)

GFP

A

D

G

α-SMA

B

E

H

Merge

C

F

I GFP/α-SMA/DAPI

ASC + αSMA

ASC - αSMA

endogenous cell + αSMA
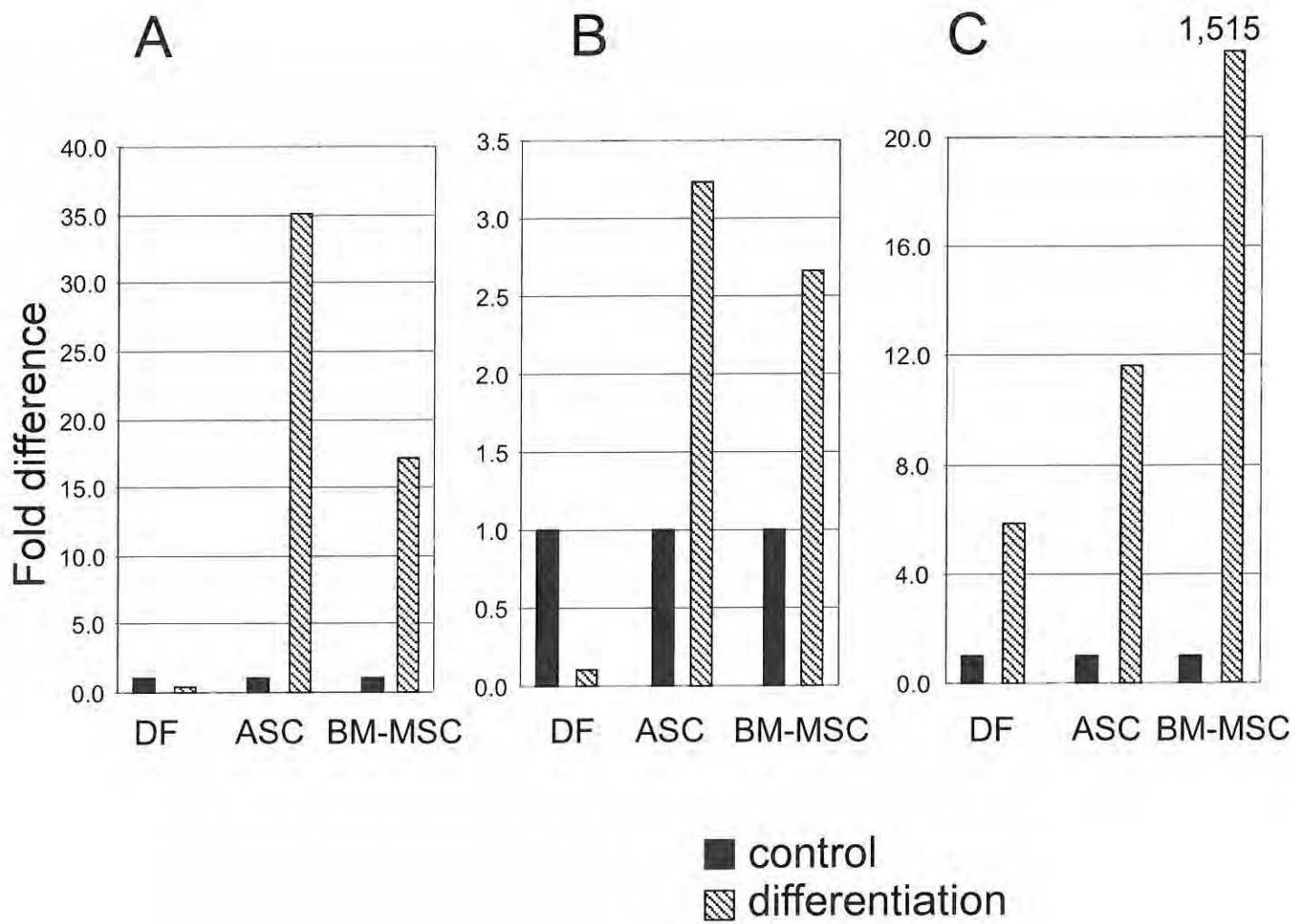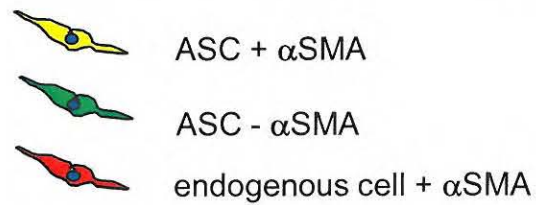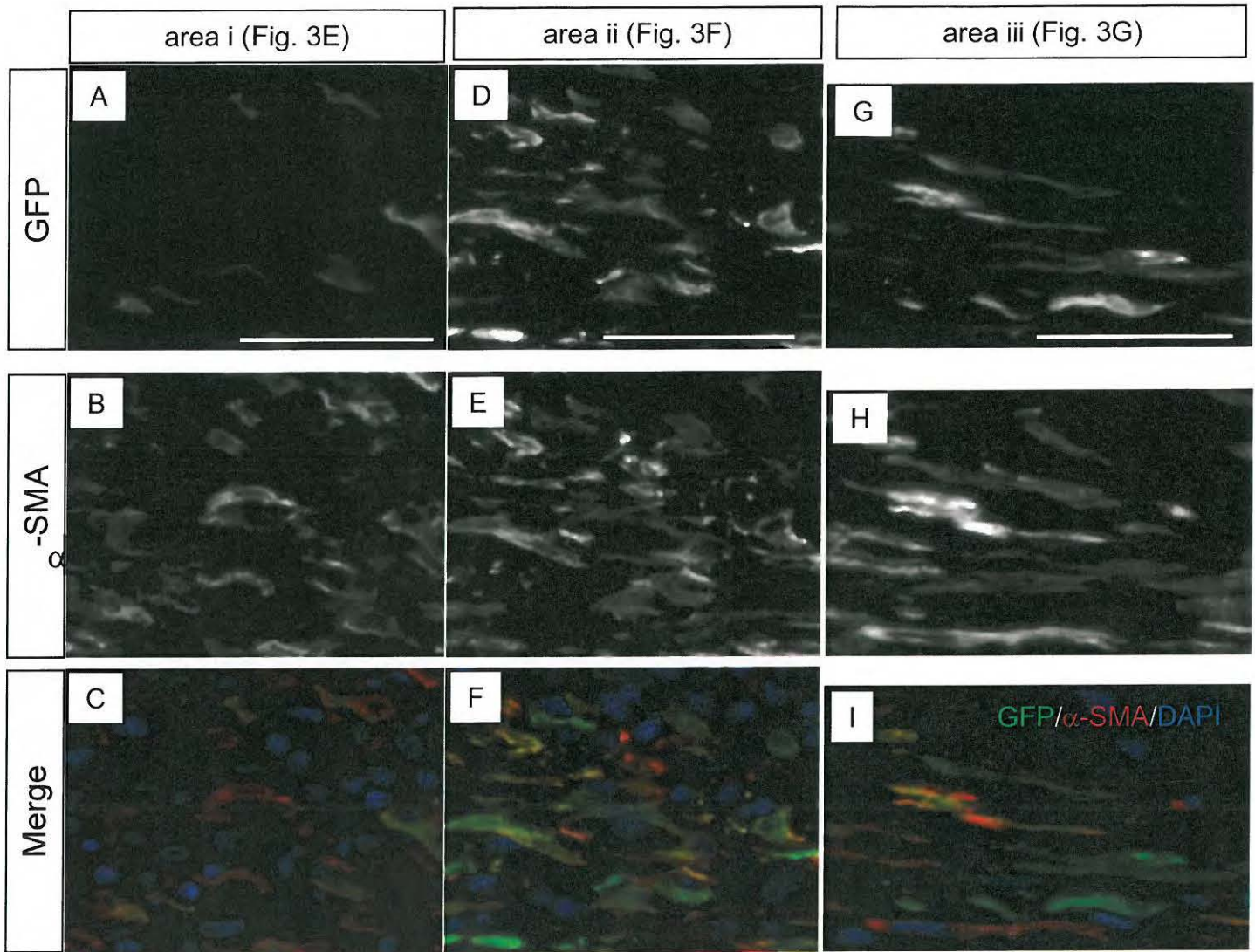
Supplemental Figure S3

Supplemental Figure S4

	section 1	section 2
GFP	A	D
CD31	B	E
Merge	C GFP/CD31/DAPI	F GFP/CD31/DAPI
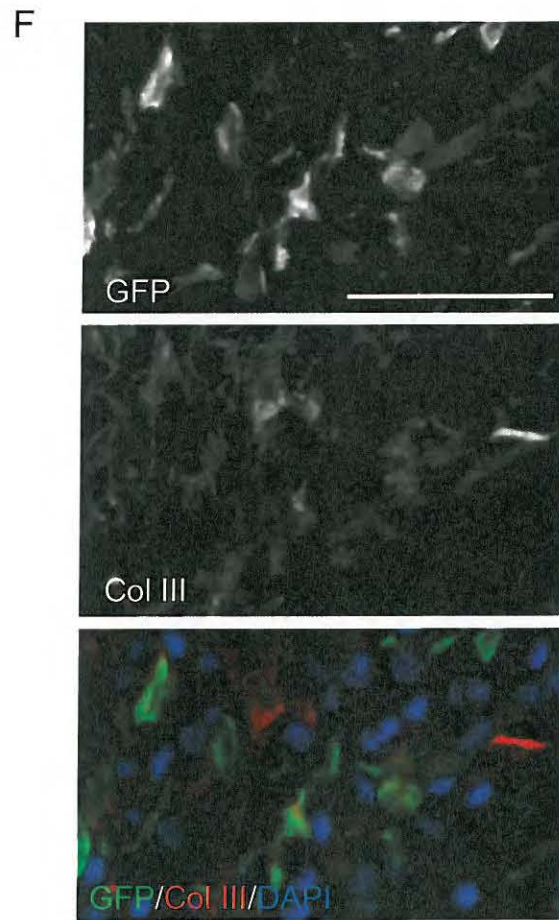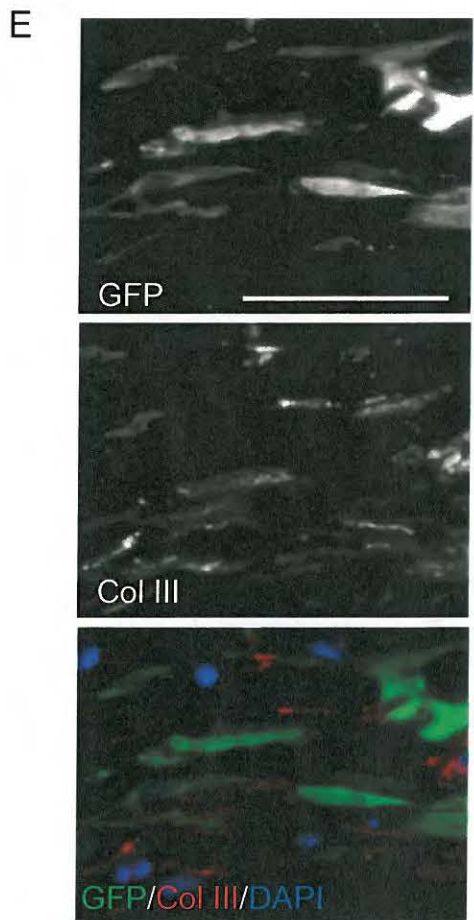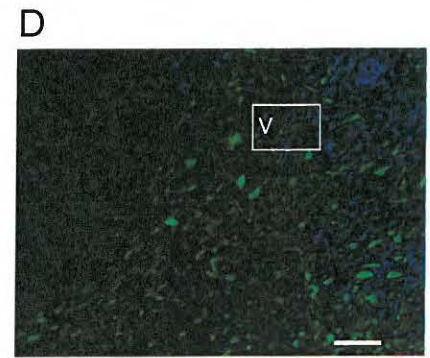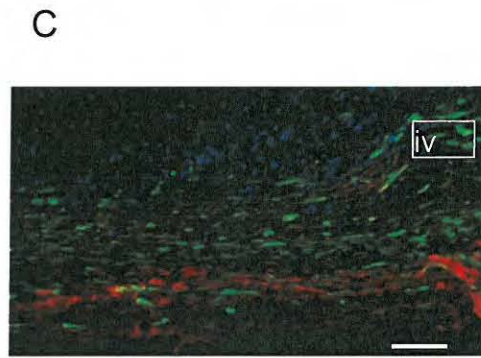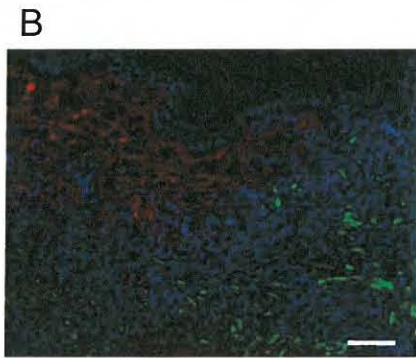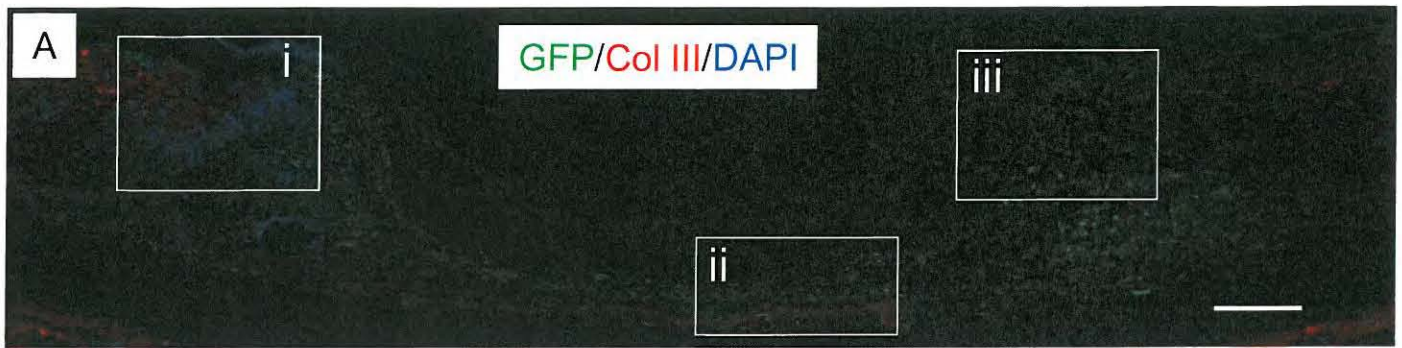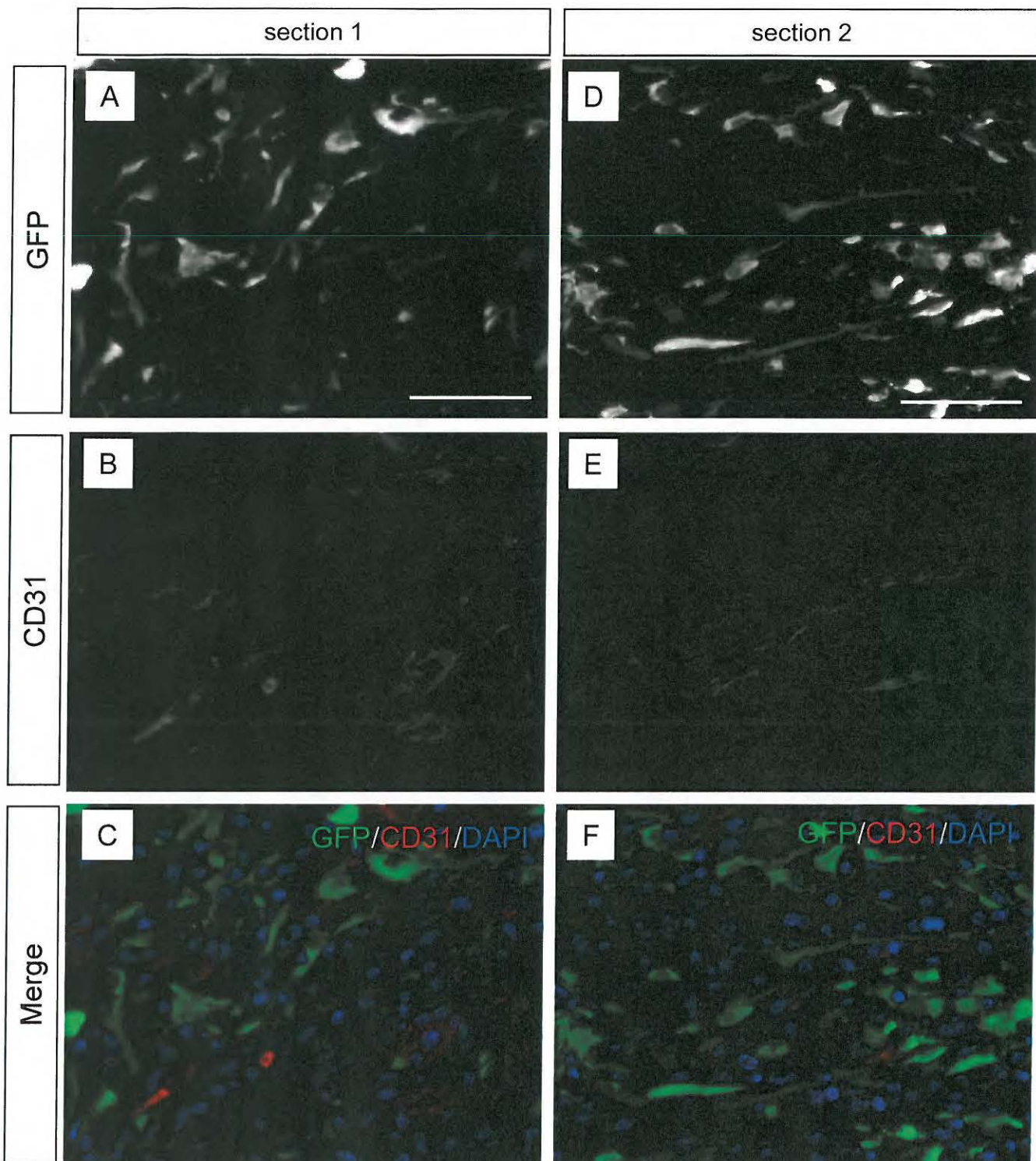
Supplemental Figure S5

Supplemental Figure S6

half wound

GA

EG

ventral skin →

cartilage →

dorsal skin →

7 mm

old (unwounded) tissue

cartilage defect from punch

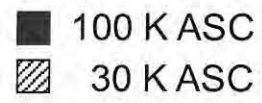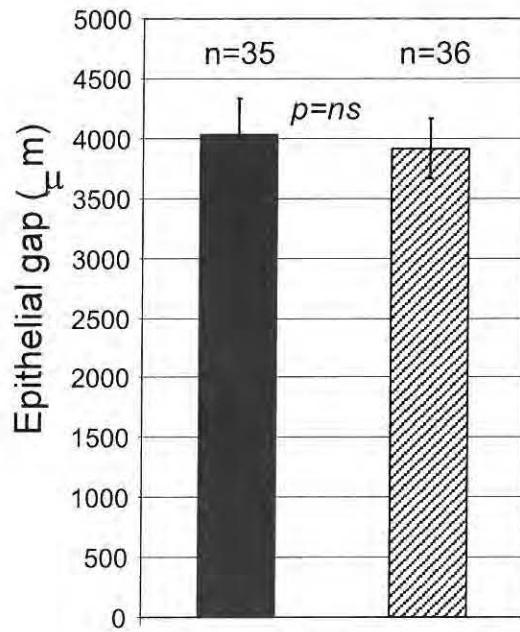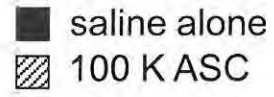Supplemental Figure S7

Supplemental Figure S8

Supplemental Figure S9